

**A POSTERIORI ERROR CONTROL & ADAPTIVITY  
FOR CRANK-NICOLSON FINITE ELEMENT APPROXIMATIONS  
FOR THE LINEAR SCHRÖDINGER EQUATION**

THEODOROS KATSAOUNIS AND IRENE KYZA

**ABSTRACT.** We derive optimal order a posteriori error estimates for fully discrete approximations of linear Schrödinger-type equations, in the  $L^\infty(L^2)$ -norm. For the discretization in time we use the Crank-Nicolson method, while for the space discretization we use finite element spaces that are allowed to change in time. The derivation of the estimators is based on a novel elliptic reconstruction that leads to estimates which reflect the physical properties of Schrödinger equations. The final estimates are obtained using energy techniques and residual-type estimators. Various numerical experiments for the one-dimensional linear Schrödinger equation in the semiclassical regime, verify and complement our theoretical results. The numerical implementations are performed with both uniform partitions and adaptivity in time and space. For adaptivity, we further develop and analyze an existing time-space adaptive algorithm to the cases of Schrödinger equations. The adaptive algorithm reduces the computational cost substantially and provides efficient error control for the solution and the observables of the problem, especially for small values of the Planck constant.

1. INTRODUCTION

In this paper we focus on the a posteriori error control and adaptivity for fully discrete Crank-Nicolson finite element (CNFE) schemes for the general form of linear Schrödinger equation:

$$(1.1) \quad \begin{cases} \partial_t u - i\alpha \Delta u + ig(x, t)u = f(x, t) & \text{in } \Omega \times (0, T], \\ u = 0 & \text{on } \partial\Omega \times (0, T], \\ u(\cdot, 0) = u_0 & \text{in } \Omega, \end{cases}$$

where  $\Omega$  is a convex “polygonal” domain in  $\mathbb{R}^d$ ,  $1 \leq d \leq 3$ , with boundary  $\partial\Omega$ , and  $0 < T < \infty$ . In (1.1),  $\alpha$  is a positive constant,  $g : \Omega \times (0, T] \rightarrow \mathbb{R}$  and  $f : \Omega \times (0, T] \rightarrow \mathbb{C}$  are given functions and  $u_0 : \Omega \rightarrow \mathbb{C}$  is a given initial value.

A special case of (1.1) is the so-called linear Schrödinger equation in the semiclassical regime:

$$(1.2) \quad \partial_t u - i\frac{\varepsilon}{2}\Delta u + \frac{i}{\varepsilon}V(x, t)u = 0,$$

with high frequency initial data. It is clear that (1.2) can be obtained from (1.1) by setting  $\alpha := \frac{\varepsilon}{2}$ ,  $g := \frac{1}{\varepsilon}V$  and  $f \equiv 0$ . In (1.2),  $\varepsilon$  ( $0 < \varepsilon \ll 1$ ) is the scaled Planck constant,  $V$  is an  $L^\infty(L^\infty)$  time-dependent potential and  $u$  is the wave function. The wave function  $u$  is used to define primary physical quantities, called *observables* ([2, 16]), such as the *position density*,

$$(1.3) \quad N(x, t) := |u(x, t)|^2,$$

and the *current density*,

$$(1.4) \quad J(x, t) := \text{Im} \left( \overline{u(x, t)} \nabla u(x, t) \right).$$

Problems related to (1.2) are of great interest in physics and engineering. However, the solution of (1.2) is complicated from the theoretical as well as the numerical analysis point of view. It is well known that for  $\varepsilon$  small (close to zero), the solution of (1.2) oscillates with wavelength  $\mathcal{O}(\varepsilon)$ , preventing  $u$  to converge strongly as  $\varepsilon \rightarrow 0$ . Because of this, standard numerical methods fail to correctly approximate  $u$  and the observables, unless very fine mesh sizes and time steps are used. In particular, previous works (cf., e.g., [2, 26, 27]) suggested

---

*Date:* April 19, 2022.

*Key words and phrases.* A posteriori error estimates, adaptive algorithm, Crank-Nicolson finite element schemes, linear Schrödinger equations, modified elliptic reconstruction, time-space reconstructions.

The research of I.K. was supported by the European Social Fund (ESF) -European Union (EU) and National Resources of the Greek State within the framework of the Action “Supporting Postdoctoral Researchers” of the Operational Programme “Education and Lifelong Learning (EdLL)”. Th. Katsaounis was partially supported by European Union FP7 program Capacities (Regpot 2009-1), through ACMAC (<http://www.acmac.uoc.gr>).

that for standard finite element (FE) methods there is a very restrictive dispersive relation connecting the mesh sizes (space and time) with parameter  $\varepsilon$ ; cf., e.g., (4.9) below. This restrictive dispersive relation can be relaxed using the so-called time-splitting spectral methods, introduced earlier by Bao, Jin & Markowich in [2], for the approximation of the solution of (1.2).

In this paper, our goal is to show that constructing adaptive algorithms based on rigorous a posteriori error control leads to CNFE schemes which are competitive to the best available methods for the approximation of the solution (and the observables) of the semiclassical Schrödinger equation (1.2), and in general of linear Schrödinger equations of the form (1.1). It also permits, for the first time, realistic computations for rough potentials for the linear Schrödinger equation in the semiclassical regime. To achieve our goal, in the current work we:

- Provide rigorous a posteriori error analysis for (1.1) for CNFE approximations using FE spaces that are allowed to change in time;
- Study the advantages of adaptivity through the obtained estimators for the efficient error control of (1.1).

Optimal order a posteriori error estimates for the heat equation for CNFE schemes with FE spaces that are allowed to change in time have been derived very recently by Bänsch, Karakatsani & Makridakis in [5]. However the extension of those ideas from the simple heat equation to the linear Schrödinger equation (1.1) is of increased difficulty due to the complex-value and multiscale nature of the problem. Because of this, novel ideas and techniques are introduced. More precisely, our main contributions are:

- Derivation of optimal order a posteriori error bounds in the  $L^\infty(L^2)$ -norm for CNFE schemes for (1.1). The fact that the analysis includes time-dependent potentials, makes the problem more challenging since there are no rigorous results for Schrödinger equations for such potentials. In addition the existing literature on a posteriori error analysis for problems with time-dependent operators of the form  $\mathcal{A}(t) := -\alpha\Delta + g(x, t)$  is quite limited. To the best of our knowledge, only in [7] the authors consider similar operators. Moreover the derived estimates hold for  $L^\infty(L^\infty)$ -type potentials as well, in contrast to the existing literature. In particular, existing results require smooth  $C^1(C^2)$ -type potentials. However, this regularity requirement on the potential is rather restrictive from applications' point of view. Including  $L^\infty(L^\infty)$  time-dependent potentials in the analysis is important for another reason: It can be considered as the first step for the a posteriori error control of nonlinear Schrödinger (NLS) equations. More precisely, the relaxation scheme introduced by Besse in [3] suggests that a posteriori error bounds for linear Schrödinger equations with  $L^\infty(L^\infty)$ -type time-dependent potentials is essential for the efficient approximation of the solution of certain NLS equations.
- Introduction of a *novel elliptic reconstruction* leading to upper bounds that do not involve the global  $L^\infty(L^\infty)$ -norm of  $g$ , and thus, to bounds that do reflect the physical properties of the problem. The elliptic reconstruction was developed by Makridakis & Nochetto in [24] to derive optimal order  $L^\infty(L^2)$  a posteriori error bounds for FE spatial discrete schemes for the heat equation using energy techniques. A straightforward generalization of this notion of the elliptic reconstruction to Schrödinger equations leads to estimates that involve the  $L^\infty(L^\infty)$ -norm of the potential. Consequently, the obtained estimates are practically useless and adaptivity is inefficient, even in the simplest case of constant potentials. Therefore, proposing a modified elliptic reconstruction based on the physical properties of the problem under consideration is crucial for the efficient error control of (1.1) (and so (1.2)). Additionally, the new ideas developed for this purpose might be useful for other problems as well, such as convection-diffusion or reaction-diffusion problems.
- A detailed numerical study on the reliability and robustness of the a posteriori estimators through a *time-space adaptive algorithm*. Our starting point is the adaptive algorithm proposed in [28], adapted to the linear Schrödinger equation, (1.2). The a posteriori estimators derived in this work are on the solution  $u$  of (1.1). However, in many applications observables like the position density (1.3), or the current density (1.4) are far more important than the solution itself. Thus, we introduce an appropriate modification of the a posteriori estimators and the adaptive algorithm. This modification is based on a heuristic idea and the results concerning the observables are very encouraging. Overall, the adaptive algorithm reduces the computational cost substantially and provides efficient error control of  $u$  and the observables for small values of the Planck constant  $\varepsilon$ . It is very difficult to obtain such results via standard techniques and without adaptivity. We point out that our purpose is not to prove convergence and optimality of the considered time-space adaptive algorithm, but rather to show that adaptivity based on rigorous a posteriori error control can be proven beneficial for the approximation of the solution (and the observables) of the linear semiclassical Schrödinger equation (1.2). In addition, it is to be emphasized that as long as the adaptive

algorithm converges, we can guarantee rigorously, based on the a posteriori error analysis, that *total error remains below a given tolerance*.

For parabolic problems, a number of adaptive algorithms exists in the literature; cf., e.g., [9, 30] and the references therein. However, convergence and optimality of time-space adaptive algorithms are very delicate and difficult issues. In the literature exists only one proven convergent time-space adaptive algorithm for evolution problems and can be found in [17]. This algorithm is appropriate for the heat equation and backward Euler FE schemes and it is not clear how to generalize it to other problems and higher order in time methods.

Despite the fact that problem (1.1) (and thus (1.2)) is linear, a posteriori error bounds and adaptive algorithms for linear Schrödinger equations are very limited in the literature. In particular, a posteriori error estimates in the  $L^\infty(L^2)$ -norm for fully discrete CNFE schemes have been proven earlier by Dörfler in [13]; these estimates are first order accurate in time, thus not optimal. Using these estimates, Dörfler also proposes an adaptive algorithm in [13]. In [18] (see also [19]), we considered only time-discrete approximations and we managed to prove optimal order a posteriori error estimates for (1.1) in the  $L^\infty(L^2)$  and  $L^\infty(H^1)$ -norms. This was achieved using the Crank-Nicolson reconstruction proposed by Akrivis, Makridakis & Nochetto in [1]. Similar estimates for (1.1), using an alternative reconstruction, proposed by Lozinski, Picasso & Prachittham in [23], can be found in [19]. To the best of our knowledge, optimal order a posteriori error estimates for fully discrete CNFE schemes do not exist in the literature. Some preliminary results to that direction can be found in [19]. However, the a posteriori estimators derived in [19] are scaled by the global  $L^\infty(L^\infty)$ -norm of  $g$ . Hence, as already mentioned, the derived estimators do not reflect the physical properties of the problem, which makes adaptivity through these estimates not reliable.

A posteriori error estimates in the  $L^\infty(L^2)$ -norm have been proven earlier in [20] for uniform partitions and the time-splitting spectral methods for the linear Schrödinger equation in the semiclassical regime (1.2). In [20], only the one-dimensional case in space is studied and the analysis, as in [2], permits only time-independent potentials, without being obvious how the theory can be extended to time-dependent potentials. In addition, the time-spectral methods require smooth potentials; the particular analysis is not applicable for  $L^\infty(L^\infty)$ -type potentials.

The analysis of the current paper is based on the introduction of appropriate space-time reconstructions. Such reconstructions for CNFE methods and FE spaces that are allowed to change in time were introduced, for the first time, very recently, by Bänsch, Karakatsani & Makridakis in [5], for the proof of optimal order a posteriori estimates in the  $L^\infty(L^2)$ -norm for the heat equation. To define those time-space reconstructions, the authors combined the idea of the elliptic reconstruction in [24] with the Crank-Nicolson reconstruction of [1, 23]. The notion of the elliptic reconstruction has also been used earlier in [21] and [15] for the derivation of optimal order a posteriori error estimates for backward Euler FE schemes for the heat and the wave equation, respectively. The reconstruction technique is a useful tool for deriving optimal order a posteriori error bounds; usually, this is not feasible via a direct comparison of the exact and the numerical solution; cf., e.g., [13, 33]. In our context, time-space reconstructions can be defined through the novel elliptic reconstruction we introduce and the Crank-Nicolson reconstruction of [1].

More precisely, the paper is organized as follows. In Section 2, we introduce notation, the variational formulation of problem and the fully discrete scheme. We propose the novel elliptic reconstruction and discuss its properties. With the aim of this new elliptic reconstruction, we then define appropriate time-space reconstructions. The main theoretical results are stated in Section 3, where the a posteriori analysis is developed and optimal order error bounds are derived using energy techniques, residual-type error estimators and the properties of the reconstructions. The two last sections are devoted to the numerical investigation of the efficiency of the estimators. In particular, in Section 4, we validate numerically the optimal order of convergence of the estimators using uniform partitions. For the linear Schrödinger equation in the semiclassical regime, we verify numerically that the estimators have the expected behavior with respect to the scaled parameter  $\varepsilon$ . Finally, in Section 5, we appropriately modify and apply to the one-dimensional semiclassical Schrödinger equation a time-space adaptive algorithm described in [9, 30] (see also [28]). We further develop the algorithm and we make it applicable for the approximation not only of the exact solution  $u$  but also for the observables, and we discuss in detail the benefits of adaptivity for equations of the form (1.2).

## 2. PRELIMINARIES

**2.1. The continuous problem.** Problem (1.1) can be rewritten equivalently in variational form as

$$(2.1) \quad \begin{cases} \langle \partial_t u(t), v \rangle + i\alpha \langle \nabla u(t), \nabla v \rangle + i \langle g(t)u(t), v \rangle = \langle f(t), v \rangle, & \forall v \in H_0^1(\Omega), t \in [0, T], \\ u(\cdot, 0) = u_0 & \text{in } \bar{\Omega}, \end{cases}$$

where  $\langle \cdot, \cdot \rangle$  denotes the  $L^2$ -inner product, or the  $H^{-1} - H_0^1$  duality pairing, depending on the context. We also denote by  $\|\cdot\|$  the norm in  $L^2(\Omega)$ . It is well known that, if  $g \in C^1([0, T]; C^1(\overline{\Omega}))$ ,  $f \in L^2([0, T]; L^2(\Omega))$ ,  $f_t \in L^2([0, T]; H^{-1}(\Omega))$ , and  $u_0 \in H_0^1(\Omega)$ , then problem (2.1) admits a unique weak solution  $u \in C([0, T]; H_0^1(\Omega))$  with  $u_t \in C([0, T]; H^{-1}(\Omega))$ ; cf., e.g., [29, 11, pages 620–630]. We thus assume that the data of (1.1) have the necessary regularity to guarantee the existence of a unique weak solution of (2.1). We emphasize that the a posteriori error estimates derived in the sequel, remain valid for  $g \in L^\infty(\Omega \times (0, T))$  as well, provided that (1.1) is well-posed. In other words, in contrast to the existing analyses, ours includes rough potentials as well, under the knowledge of the well-posedness of (1.1). To avoid making the forthcoming analysis more technical, we further assume that  $g$  satisfies

$$(2.2) \quad \sup_{x \in \Omega} g(x, t) \geq - \inf_{x \in \Omega} g(x, t), \quad \forall t \in [0, T].$$

Condition (2.2) is not restrictive from applications' point of view, as, in most applications,  $g$  denotes a non-negative potential and thus (2.2) is automatically satisfied.

**2.2. The method.** We consider a partition  $0 =: t_0 < t_1 < \dots < t_N := T$  of  $[0, T]$ , and let  $I_n := (t_{n-1}, t_n]$  and  $k_n := t_n - t_{n-1}$ ,  $1 \leq n \leq N$ , denote the subintervals of  $[0, T]$  and the time steps, respectively. Let also  $k := \max_{1 \leq n \leq N} k_n$ . We discretize (1.1) by a Galerkin finite element method. To this end, we introduce a family  $\{\mathcal{T}_n\}_{n=0}^N$  of conforming shape-regular triangulations of  $\Omega$ . We further assume that each triangulation  $\mathcal{T}_n$ ,  $1 \leq n \leq N$ , is a refinement of a macro-triangulation of  $\Omega$  and that  $\mathcal{T}_{n-1}$  and  $\mathcal{T}_n$  are compatible. Two triangulations are said to be compatible if they are derived from the same macro-triangulation by an admissible refinement procedure. For precise definitions of these properties of the family  $\{\mathcal{T}_n\}_{n=0}^N$ , we refer to [21, 12]. Note that the triangulations are allowed to change arbitrarily from one step to another, provided they satisfy the aforementioned compatibility conditions. These conditions are minimal and allow for heavily graded meshes and adaptivity. Additionally, the forthcoming analysis is applicable without any quasiniformity type assumptions on the mesh and without any restrictions on the sizes of neighboring elements of the triangulation.

For an element  $K \in \mathcal{T}_n$ , we denote its boundary by  $\partial K$ . Let  $h_K$  be the diameter of  $K \in \mathcal{T}_n$  and  $h := \max_{0 \leq n \leq N} \max_{K \in \mathcal{T}_n} h_K$ . Let also  $\Sigma_n(K)$  be the set of internal sides of  $K \in \mathcal{T}_n$  (points in  $d = 1$ , edges in  $d = 2$  and faces in  $d = 3$ ) and define  $\Sigma_n := \bigcup_{K \in \mathcal{T}_n} \Sigma_n(K)$ . To any side  $e \in \Sigma_n$ , we associate a unit vector  $\mathbf{n}_e$  on  $e$  and for  $x \in e$  and a function  $v$ , we define

$$J[\nabla v](x) := \lim_{\delta \rightarrow 0} \left[ \nabla v(x + \delta \mathbf{n}_e) - \nabla v(x - \delta \mathbf{n}_e) \right] \cdot \mathbf{n}_e.$$

To each triangulation  $\mathcal{T}_n$ , we associate the finite element space  $\mathbb{V}^n$ ,

$$\mathbb{V}^n := \{\Phi_n \in H_0^1(\Omega) : \forall K \in \mathcal{T}_n, \Phi_n|_K \in \mathbb{P}^r\},$$

where  $\mathbb{P}^r$  denotes the space of polynomials in  $d$  variables of degree at most  $r$ .

With  $\widehat{\mathcal{T}}_n := \mathcal{T}_n \wedge \mathcal{T}_{n-1}$  we denote the finest common coarsening triangulation of  $\mathcal{T}_n$  and  $\mathcal{T}_{n-1}$  and by  $\widehat{\mathbb{V}}^n := \mathbb{V}^n \cap \mathbb{V}^{n-1}$  its corresponding finite element space. Finally, let  $\widehat{\Sigma}_n := \Sigma_n \cup \Sigma_{n-1}$ , and for  $K \in \widehat{\mathcal{T}}_n$ , let  $\widehat{\Sigma}_K^n := \widehat{\Sigma}_n \cap K$ , where the element  $K \in \widehat{\mathcal{T}}_n$  is taken to be closed.

**Definition 2.1** (discrete Laplacian). *For  $0 \leq n \leq N$ , the discrete version  $-\Delta^n : \mathbb{V}^n \rightarrow \mathbb{V}^n$  of the Laplace operator  $-\Delta$  onto  $\mathbb{V}^n$  is defined as*

$$(2.3) \quad \langle -\Delta^n v, \Phi_n \rangle = \langle \nabla v, \nabla \Phi_n \rangle, \quad \forall \Phi_n \in \mathbb{V}^n.$$

We now discretize problem (1.1) by a *modified Crank-Nicolson-Galerkin* scheme, introduced earlier for the heat equation in [5]. Given an approximation  $U^{n-1} \in \mathbb{V}^{n-1}$  to the exact solution at  $t^{n-1}$  we define approximation  $U^n \in \mathbb{V}^n$  to the exact solution  $u$  at the nodes  $t_n$ ,  $0 \leq n \leq N$ , by the numerical method:

$$(2.4) \quad \frac{U^n - \Pi^n U^{n-1}}{k_n} - i\alpha \frac{\Pi^n \Delta^{n-1} U^{n-1} + \Delta^n U^n}{2} + i\mathcal{P}^n \left( g(t_{n-\frac{1}{2}}) U^{n-\frac{1}{2}} \right) = \mathcal{P}^n f(t_{n-\frac{1}{2}}),$$

for  $1 \leq n \leq N$ , with  $U^0 := \mathcal{P}^0 u_0$  in  $\Omega$ . In (2.4),  $t_{n-\frac{1}{2}} := \frac{t_{n-1} + t_n}{2}$ ,  $U^{n-\frac{1}{2}} := \frac{U^{n-1} + U^n}{2}$ , and  $\mathcal{P}^n : L^2(\Omega) \rightarrow \mathbb{V}^n$ ,  $\Pi^n : \mathbb{V}^{n-1} \rightarrow \mathbb{V}^n$  are appropriate projections or interpolants. In Sections 4, 5, where we discuss the numerical experiments,  $\mathcal{P}^n$  and  $\Pi^n$  are taken to be the  $L^2$ -projection. However, the theory is still valid for other choices of  $\mathcal{P}^n$  and  $\Pi^n$  (cf. [5, 6]), and therefore we consider the method in this general setting. Another non-standard term appearing in (2.4) is  $\Pi^n \Delta^{n-1} U^{n-1}$  instead of  $\Delta^n U^{n-1}$ . As it was observed in [5, 6], considering  $\Delta^n U^{n-1}$  instead of  $\Pi^n \Delta^{n-1} U^{n-1}$  may lead to oscillatory behavior of the obtained a posteriori estimators. For this reason, we consider the modified scheme (2.4) instead of the standard one.

**2.3. Novel elliptic reconstruction–Residual-type estimators.** The elliptic reconstruction was originally introduced by Makridakis & Nochetto in [24] for the proof of optimal order a posteriori error estimates in space in the  $L^\infty(L^2)$ –norm for evolution problems, using energy techniques. It was also one of the main tools in the a posteriori error analysis of the heat equation for Crank-Nicolson fully discrete schemes; cf. [5]. For the linear Schrödinger equation (1.1), we introduce a new type of elliptic reconstruction which reflects the physical properties of the problem, and in particular the physical properties of the semiclassical Schrödinger equation (1.2). To this end, we introduce, in each  $I_n$ , the constant

$$(2.5) \quad \bar{g}_n := \frac{1}{2} \left[ \sup_{x \in \Omega} g(x, t_{n-\frac{1}{2}}) + \inf_{x \in \Omega} g(x, t_{n-\frac{1}{2}}) \right].$$

The main reason for the choice of (2.5) is that the knowledge on “how far from  $\bar{g}_n$  is  $g$  in  $\Omega$ ” gives qualitative information on the behavior of the exact solution, especially in the case of linear Schrödinger equation in the semiclassical regime. In order for the elliptic reconstruction we introduce below to be well defined, we need  $\bar{g}_n \geq 0$ , which is automatically satisfied due to (2.2).

**Definition 2.2** (novel elliptic reconstruction). *For fixed  $V_n \in \mathbb{V}^n$  we define the elliptic reconstruction  $\mathcal{R}^n V_n \in H_0^1(\Omega)$  of  $V_n$  to be the weak solution of the elliptic problem*

$$(2.6) \quad \alpha \langle \nabla \mathcal{R}^n V_n, \nabla \phi \rangle + \bar{g}_n \langle \mathcal{R}^n V_n, \phi \rangle = \langle (-\alpha \Delta^n + \bar{g}_n) V_n, \phi \rangle, \quad \forall \phi \in H_0^1(\Omega).$$

As we shall see in the sequel, the above modified elliptic reconstruction will allow us to obtain qualitatively better a posteriori error estimators compared to those obtained using the standard elliptic reconstruction; cf., [19]. In fact, the  $\sup_{x \in \Omega} |g(x, t)|$  that appears in the standard results of a priori error analysis, can now be replaced, due to (2.6), by  $\sup_{x \in \Omega} |g(x, t) - \bar{g}_n|$ ,  $t \in I_n$ , leading to better constants. A very interesting question here, that needs further investigation, is whether the global constant  $\sup_{x \in \Omega} |g(x, t) - \bar{g}_n|$  can be localized in each element. This will not only lead to better constants in the final a posteriori error estimators, but also might give the inspiration of proposing appropriate adaptive strategies.

Using (2.3), we see that  $\mathcal{R}^n$  satisfies the orthogonality property

$$(2.7) \quad \alpha \langle \nabla (\mathcal{R}^n - \mathbb{I}) V_n, \nabla \Phi_n \rangle + \bar{g}_n \langle (\mathcal{R}^n - \mathbb{I}) V_n, \Phi_n \rangle = 0, \quad \forall \Phi_n \in \mathbb{V}_n.$$

Let now  $z$  be the weak solution of the following elliptic problem

$$(2.8) \quad \langle \nabla z, \nabla \phi \rangle = \langle (\mathcal{R}^n - \mathbb{I}) V_n, \phi \rangle, \quad \forall \phi \in H_0^1(\Omega),$$

and let  $\mathcal{I}_n z$  be its Clément-type interpolant in  $\mathbb{V}^n$  (for the definition of the Clément-type interpolant and its properties we refer to [4, 10, 32]). Then we can prove the next auxiliary lemma.

**Lemma 2.1.** *Let  $z$  be the solution of (2.8) and  $\mathcal{I}_n z$  its Clément-type interpolant. Then, for all  $V_n \in \mathbb{V}^n$ , we have the following estimate for  $\mathcal{R}^n V_n$*

$$(2.9) \quad \|(\mathcal{R}^n - \mathbb{I}) V_n\|^2 \leq \left| \langle -\Delta^n V_n, z - \mathcal{I}_n z \rangle - \langle \nabla V_n, \nabla (z - \mathcal{I}_n z) \rangle \right|.$$

*Proof.* Using (2.8), we obtain

$$\|(\mathcal{R}^n - \mathbb{I}) V_n\|^2 = \langle \nabla (\mathcal{R}^n - \mathbb{I}) V_n, \nabla z \rangle,$$

and thus, invoking the definition of the modified elliptic reconstruction (2.6) and the orthogonality property (2.7), we arrive at

$$\|(\mathcal{R}^n - \mathbb{I}) V_n\|^2 = \langle -\Delta^n V_n, z - \mathcal{I}_n z \rangle - \langle \nabla V_n, \nabla (z - \mathcal{I}_n z) \rangle - \frac{1}{\alpha} \bar{g}_n \langle (\mathcal{R}^n - \mathbb{I}) V_n, z \rangle.$$

Since both  $\alpha$  and  $\bar{g}_n$  are positive, (2.9) follows by  $\langle (\mathcal{R}^n - \mathbb{I}) V_n, z \rangle = \|\nabla z\|^2 \geq 0$ ; cf. (2.8).  $\square$

Since we use finite element spaces that are allowed to change from  $t_{n-1}$  to  $t_n$ , we will need to work with quantities of the form  $\|(\mathcal{R}^n - \mathbb{I}) V_n - (\mathcal{R}^{n-1} - \mathbb{I}) V_{n-1}\|$  for  $V_n \in \mathbb{V}^n$  and  $V_{n-1} \in \mathbb{V}^{n-1}$ . To estimate such a quantity, we consider the elliptic problem

$$\langle \nabla \hat{z}, \nabla \phi \rangle = \langle (\mathcal{R}^n - \mathbb{I}) V_n - (\mathcal{R}^{n-1} - \mathbb{I}) V_{n-1}, \phi \rangle, \quad \forall \phi \in H_0^1(\Omega)$$

with solution  $\hat{z}$  and we denote by  $\widehat{\mathcal{I}}_n \hat{z}$  its Clément-type interpolant onto  $\widehat{\mathbb{V}}_n$ .

**Lemma 2.2.** *For  $V_n \in \mathbb{V}^n$  and  $V_{n-1} \in \mathbb{V}^{n-1}$  we have that*

$$(2.10) \quad \begin{aligned} \|(\mathcal{R}^n - \mathbb{I}) V_n - (\mathcal{R}^{n-1} - \mathbb{I}) V_{n-1}\|^2 \leq & \left| \langle \Delta^n V_n, \hat{z} - \widehat{\mathcal{I}}_n \hat{z} \rangle - \langle \nabla V_n, \nabla (\hat{z} - \widehat{\mathcal{I}}_n \hat{z}) \rangle \right. \\ & \left. + \langle \Delta^{n-1} V_{n-1}, \hat{z} - \widehat{\mathcal{I}}_n \hat{z} \rangle + \langle \nabla V_{n-1}, \nabla (\hat{z} - \widehat{\mathcal{I}}_n \hat{z}) \rangle \right|. \end{aligned}$$

*Proof.* The proof is similar to the proof of Lemma 2.1.  $\square$

To estimate a posteriori the errors  $\|(\mathcal{R}^n - \mathbb{I})V_n\|$  and  $\|(\mathcal{R}^n - \mathbb{I})V_n - (\mathcal{R}^{n-1} - \mathbb{I})V_{n-1}\|$ , we use residual-type error estimators. To this end, for a given  $V_n \in \mathbb{V}^n$ ,  $0 \leq n \leq N$ , we define the following  $L^2$ -elliptic estimator:

$$(2.11) \quad \eta_{\mathbb{V}^n}(V_n) := \left\{ \sum_{K \in \mathcal{T}_n} \left( \|h_K^2 (\Delta - \Delta^n) V_n\|_{L^2(K)}^2 + \|h_K^{\frac{3}{2}} J[\nabla V_n]\|_{L^2(\partial K)}^2 \right) \right\}^{\frac{1}{2}}.$$

In case  $d = 1$ , the term with the discontinuities in (2.11) vanishes. For  $V_n \in \mathbb{V}^n$  and  $V_{n-1} \in \mathbb{V}^{n-1}$ ,  $1 \leq n \leq N$ , we also define

$$(2.12) \quad \eta_{\widehat{\mathbb{V}}^n}(V_n, V_{n-1}) := \left\{ \sum_{K \in \widehat{\mathcal{T}}_n} \left( \|h_K^2 [(\Delta - \Delta^n)V_n - (\Delta - \Delta^{n-1})V_{n-1}]\|_{L^2(K)}^2 + \|h_K^{\frac{3}{2}} J[\nabla V_n - \nabla V_{n-1}]\|_{L^2(\widehat{\mathcal{S}}_K^n)}^2 \right) \right\}^{\frac{1}{2}}.$$

In view of the definition of  $\eta_{\mathbb{V}^n}$  and of (2.9), the Lemma below is standard. Its proof is based on duality arguments and the elliptic regularity estimate for the Laplace operator. For details on the proof we refer, for example, to [24, 21].

**Lemma 2.3.** *For all  $V_n \in \mathbb{V}^n$ ,  $0 \leq n \leq N$ , it holds*

$$(2.13) \quad \|(\mathcal{R}^n - \mathbb{I})V_n\| \leq C \eta_{\mathbb{V}^n}(V_n),$$

where the constant  $C$  depends only on the domain  $\Omega$  and the shape regularity of the family of triangulations.  $\square$

Similarly, by (2.10) the estimate (2.14) in the next lemma holds. For a detailed proof, we refer to [21, 5].

**Lemma 2.4.** *For  $V_n \in \mathbb{V}^n$  and  $V_{n-1} \in \mathbb{V}^{n-1}$ ,  $1 \leq n \leq N$ , we have*

$$(2.14) \quad \|(\mathcal{R}^n - \mathbb{I})V_n - (\mathcal{R}^{n-1} - \mathbb{I})V_{n-1}\| \leq \widehat{C} \eta_{\widehat{\mathbb{V}}^n}(V_n, V_{n-1}),$$

where the constant  $\widehat{C}$  depends only on the domain  $\Omega$ , the shape regularity of the triangulations, and the number of bisections necessary to pass from  $\mathcal{T}_{n-1}$  to  $\mathcal{T}_n$ .  $\square$

**2.4. Space and time-space reconstructions.** We first define the continuous, piecewise linear interpolant  $U : [0, T] \rightarrow H_0^1(\Omega)$  between the nodal values  $U^{n-1}$  and  $U^n$ , i.e.,

$$(2.15) \quad U(t) := \ell_0^n(t)U^{n-1} + \ell_1^n(t)U^n, \quad t \in I_n,$$

with  $\ell_0^n(t) := \frac{t^n - t}{k_n}$  and  $\ell_1^n(t) := \frac{t - t_{n-1}}{k_n}$ ,  $t \in I_n$ . The space reconstruction of  $U$ , that was used in [21] to obtain of optimal order a posteriori error estimates for the backward Euler-Galerkin fully discrete scheme is given via

$$\omega(t) := \ell_0^n(t)\mathcal{R}^{n-1}U^{n-1} + \ell_1^n(t)\mathcal{R}^nU^n, \quad t \in I_n.$$

However, as the authors note in [1, 23] to obtain optimal order in time a posteriori error estimates for the Crank-Nicolson method, a reconstruction in time is also needed. Here, with the aid of the new elliptic reconstruction (2.6), we propose a two-point time-space reconstruction for linear Schrödinger equations and the method (2.4).

**Definition 2.3** (time-space reconstruction). *For  $1 \leq n \leq N$ , we define the two-point time-space reconstruction  $\widehat{U} : I_n \rightarrow H_0^1(\Omega)$  of the CNFE scheme (2.4) as*

$$(2.16) \quad \begin{aligned} \widehat{U}(t) := & \mathcal{R}^{n-1}U^{n-1} + \frac{t - t_{n-1}}{k_n} (\mathcal{R}^n \Pi^n U^{n-1} - \mathcal{R}^{n-1}U^{n-1}) - i\alpha \int_{t_{n-1}}^t \mathcal{R}^n \Theta(s) ds \\ & - i \int_{t_{n-1}}^t \mathcal{R}^n \mathcal{P}^n G_U(s) ds + \int_{t_{n-1}}^t \mathcal{R}^n \mathcal{P}^n F(s) ds, \quad t \in I_n, \end{aligned}$$

where

$$(2.17) \quad G_U(t) := g(t_{n-\frac{1}{2}})U^{n-\frac{1}{2}} + \frac{2}{k_n} (t - t_{n-\frac{1}{2}}) \left[ g(t_{n-\frac{1}{2}})U^{n-\frac{1}{2}} - g(t_{n-1})U^{n-1} \right]$$

and

$$(2.18) \quad F(t) := f(t_{n-\frac{1}{2}}) + \frac{2}{k_n} (t - t_{n-\frac{1}{2}}) \left[ f(t_{n-\frac{1}{2}}) - f(t_{n-1}) \right],$$

denote the linear interpolants of  $gU$  and  $f$ , respectively, at the nodes  $t_{n-1}$  and  $t_{n-\frac{1}{2}}$ , and

$$(2.19) \quad \Theta(t) := \ell_0^n(t) \Pi^n(-\Delta^{n-1})U^{n-1} + \ell_1^n(t)(-\Delta^n)U^n.$$

In order to write compactly method (2.4) and the reconstruction  $\widehat{U}$ , we introduce the notation

$$(2.20) \quad W(t) := \left( i\alpha\Theta + i\mathcal{P}^n G_U - \mathcal{P}^n F \right)(t), \quad t \in I_n.$$

With this notation, the reconstruction  $\widehat{U}$  is rewritten as

$$(2.21) \quad \widehat{U}(t) = \mathcal{R}^{n-1}U^{n-1} + \frac{t-t_{n-1}}{k_n} (\mathcal{R}^n \Pi^n U^{n-1} - \mathcal{R}^{n-1}U^{n-1}) - \int_{t_{n-1}}^t \mathcal{R}^n W(s) ds, \quad t \in I_n,$$

and method (2.4) as

$$(2.22) \quad \frac{U^n - \Pi^n U^{n-1}}{k_n} + W(t_{n-\frac{1}{2}}) = 0, \quad 1 \leq n \leq N.$$

Note that in each  $[t_{n-1}, t_n]$ ,  $W$  is a linear polynomial between the values  $(t_{n-1}, W(t_{n-1}))$  and  $(t_{n-\frac{1}{2}}, W(t_{n-\frac{1}{2}}))$ . Thus, it is straightforward to see that

$$(2.23) \quad W(t) - W(t_{n-\frac{1}{2}}) = (t - t_{n-\frac{1}{2}}) \partial_t W(t), \quad t \in I_n.$$

**Proposition 2.1.** *For  $1 \leq n \leq N$ , there holds*

$$\widehat{U}(t_{n-1}^+) = \mathcal{R}^{n-1}U^{n-1} \quad \text{and} \quad \widehat{U}(t_n) = \mathcal{R}^n U^n.$$

In particular,  $\widehat{U}$  is continuous in time. Furthermore, it satisfies

$$(2.24) \quad \partial_t \widehat{U} + i\alpha \mathcal{R}^n \Theta + i\mathcal{R}^n \mathcal{P}^n G_U = \mathcal{R}^n \mathcal{P}^n F + \frac{\mathcal{R}^n \Pi^n U^{n-1} - \mathcal{R}^{n-1}U^{n-1}}{k_n} \quad \text{in } I_n.$$

*Proof.* That  $\widehat{U}(t_{n-1}^+) = \mathcal{R}^{n-1}U^{n-1}$  is obvious from the definition of  $\widehat{U}$ . Moreover,

$$\widehat{U}(t_n) = \mathcal{R}^n \Pi^n U^{n-1} - \mathcal{R}^n \int_{I_n} W(t) dt.$$

Since  $W$  is a linear polynomial in time in  $I_n$ , we have that  $\int_{I_n} W(t) dt = k_n W(t_{n-\frac{1}{2}})$  and that  $\widehat{U}(t_n) = \mathcal{R}^n U^n$  follows invoking (2.22). Finally, (2.24) is an immediate consequence of differentiation in time of (2.16).  $\square$

We conclude the section by computing the difference  $\widehat{U} - \omega$ . For this, we introduce, for  $1 \leq n \leq N$ , the notation

$$(2.25) \quad \bar{\partial} W^{n-\frac{1}{2}} := \frac{2}{k_n} \left[ W(t_{n-\frac{1}{2}}) - W(t_{n-1}) \right].$$

**Lemma 2.5** (the difference  $\widehat{U} - \omega$ ). *The difference  $\widehat{U} - \omega$  satisfies*

$$(2.26) \quad (\widehat{U} - \omega)(t) = \frac{1}{2} (t_n - t)(t - t_{n-1}) \mathcal{R}^n \bar{\partial} W^{n-\frac{1}{2}}, \quad t \in I_n.$$

*Proof.* Using the definitions of  $\widehat{U}$  and  $\omega$  and the method in the form (2.22) we obtain

$$\partial_t (\widehat{U} - \omega)(t) = -\mathcal{R}^n \left( W(t) - W(t_{n-\frac{1}{2}}) \right).$$

Thus, using (2.23) and the fact that  $\int_{t_{n-1}}^t (s - t_{n-\frac{1}{2}}) ds = \frac{1}{2} (t - t_{n-1})(t - t_n)$ , we obtain

$$(2.27) \quad (\widehat{U} - \omega)(t) = \frac{1}{2} (t_n - t)(t - t_{n-1}) \mathcal{R}^n \partial_t W(t), \quad t \in I_n.$$

Equality (2.26) follows now from (2.27), by noting that  $\partial_t W(t) = \bar{\partial} W^{n-\frac{1}{2}}$ ,  $t \in I_n$ ; cf. (2.25) and the definition (2.20) of  $W(t)$ .  $\square$

### 3. A POSTERIORI ERROR ESTIMATES IN THE $L^\infty(L^2)$ -NORM

**3.1. Main Ideas.** In this section, we establish a posteriori error estimates in the  $L^\infty(L^2)$ -norm for problem (1.1), using the tools developed in the previous section. To this end, we denote by  $e := u - U$  the error, where recall that  $U$  is the piecewise linear interpolant between the nodal values  $U^{n-1}$  and  $U^n$ ; cf. (2.15). To achieve proving optimal order a posteriori error estimates in the  $L^\infty(L^2)$ -norm for (1.1) we split the error as

$$e := \hat{\rho} + \sigma + \epsilon,$$

with  $\hat{\rho} := u - \widehat{U}$ ,  $\sigma := \widehat{U} - \omega$  and  $\epsilon := \omega - U$ . We refer to  $\hat{\rho}$  as the main error, to  $\sigma$  as the time-reconstruction error and to  $\epsilon$  as the elliptic-reconstruction error. The term  $\sigma$  measures the error due to the reconstruction in time. This term is of optimal order in time, cf. (2.26), but not yet an a posteriori quantity. It can be estimated a posteriori using the residual-type error estimators. The residual estimators will also be used for the direct estimation of the elliptic-reconstruction error.

Finally, as we shall see, the main error  $\hat{\rho}$  satisfies a perturbation of the original PDE and it will be bounded by the perturbed terms using energy techniques. The perturbed terms are either a posteriori quantities of optimal order, or can be estimated a posteriori by estimators of optimal order. These terms will include quantities that measure the time and space errors, the effect of mesh changes and the variation of the data  $f$  and  $g$ . We now proceed with the estimation of  $\sigma$  and  $\epsilon$  in Propositions 3.1 and 3.2, respectively.

**Proposition 3.1** (estimation of the time-reconstruction error). *For  $1 \leq m \leq N$ , the following estimate is valid for the time reconstruction error  $\sigma = \widehat{U} - \omega$ :*

$$(3.1) \quad \max_{0 \leq t \leq t_m} \|\sigma(t)\| \leq \mathcal{E}_m^{\text{T},0} \quad \text{with} \quad \mathcal{E}_m^{\text{T},0} := \max_{1 \leq n \leq m} \frac{k_n^2}{8} \left[ \|\bar{\partial}W^{n-\frac{1}{2}}\| + C\eta_{V^n}(\bar{\partial}W^{n-\frac{1}{2}}) \right].$$

*Proof.* We write  $\mathcal{R}^n \bar{\partial}W^{n-\frac{1}{2}} = \bar{\partial}W^{n-\frac{1}{2}} + (\mathcal{R}^n - \text{I})\bar{\partial}W^{n-\frac{1}{2}}$  and the desirable result now follows using (2.13) and (2.26).  $\square$

**Proposition 3.2** (estimation of the elliptic error). *For the elliptic error  $\epsilon = \omega - U$  we have, for  $1 \leq m \leq N$ :*

$$(3.2) \quad \max_{0 \leq t \leq t_m} \|\epsilon(t)\| \leq C\mathcal{E}_m^{\text{S},0} \quad \text{with} \quad \mathcal{E}_m^{\text{S},0} := \max_{0 \leq n \leq m} \eta_{V^n}(U^n).$$

*Proof.* For  $t \in I_n$ ,  $\epsilon = \ell_0^n(t)(\mathcal{R}^{n-1} - \text{I})U^{n-1} + \ell_1^n(t)(\mathcal{R}^n - \text{I})U^n$ . Hence,

$$\|\epsilon(t)\| \leq \max \left\{ \|(\mathcal{R}^{n-1} - \text{I})U^{n-1}\|, \|(\mathcal{R}^n - \text{I})U^n\| \right\}, \quad t \in I_n,$$

from where we immediately conclude (3.2), in view of (2.13).  $\square$

**3.2. Estimation of the main error.** In view of (2.24) we see that the reconstruction  $\widehat{U}$  satisfies, for  $t \in I_n$ , the equation

$$(3.3) \quad \langle \partial_t \widehat{U}(t), \phi \rangle + i\alpha \langle \nabla \widehat{U}(t), \nabla \phi \rangle + i \langle g(t) \widehat{U}(t), \phi \rangle = \langle R(t), \phi \rangle, \quad \forall \phi \in H_0^1(\Omega),$$

with

$$(3.4) \quad R(t) := -\mathcal{R}^n W(t) + \frac{\mathcal{R}^n \Pi^n U^{n-1} - \mathcal{R}^{n-1} U^{n-1}}{k_n} + i(-\alpha \Delta + g(t))(\omega + \sigma)(t), \quad t \in I_n.$$

**Proposition 3.3** (error equation for  $\hat{\rho}$ ). *The main error  $\hat{\rho} = u - \widehat{U}$  satisfies, for  $t \in I_n$ , the equation*

$$(3.5) \quad \langle \partial_t \hat{\rho}(t), \phi \rangle + i\alpha \langle \nabla \hat{\rho}(t), \nabla \phi \rangle + i \langle g(t) \hat{\rho}(t), \phi \rangle = \sum_{j=1}^4 \langle R_j(t), \phi \rangle, \quad \forall \phi \in H_0^1(\Omega),$$

where the residuals  $R_j$ ,  $1 \leq j \leq 4$ , are given by

$$(3.6) \quad R_1(t) := (\mathcal{R}^n - \text{I})W(t) - \frac{\mathcal{R}^n \Pi^n U^{n-1}}{k_n} + i\alpha \ell_0^n(t)(\text{I} - \Pi^n)\Delta^{n-1}U^{n-1},$$

$$(3.7) \quad R_2(t) := \frac{i}{2}(t_n - t)(t - t_{n-1}) \left[ (-\alpha \Delta^n + g(t))\bar{\partial}W^{n-\frac{1}{2}} + (g(t) - \bar{g}_n)(\mathcal{R}^n - \text{I})\bar{\partial}W^{n-\frac{1}{2}} \right],$$

$$(3.8) \quad R_3(t) := i(g(t) - \bar{g}_n) \left[ \ell_0^n(t)(\text{I} - \mathcal{R}^{n-1})U^{n-1} + \ell_1^n(t)(\text{I} - \mathcal{R}^n)U^n \right],$$

and

$$(3.9) \quad R_4(t) := i(\mathcal{P}^n G_U(t) - (gU)(t)) + (f(t) - \mathcal{P}^n F(t)).$$



*Proof.* Subtracting (3.3) from (2.1) we obtain, for  $t \in I_n$ ,

$$(3.10) \quad \langle \partial_t \hat{\rho}(t), \phi \rangle + i\alpha \langle \nabla \hat{\rho}(t), \nabla \phi \rangle + i \langle g(t) \hat{\rho}(t), \phi \rangle = \langle f(t), \phi \rangle - \langle R(t), \phi \rangle, \quad \forall \phi \in H_0^1(\Omega).$$

We further write

$$(-\alpha \Delta + g(t))\omega(t) = (-\alpha \Delta + \bar{g}_n)\omega(t) + (g(t) - \bar{g}_n)\omega(t),$$

where we recall that  $\omega(t) = \ell_0^n(t)\mathcal{R}^{n-1}U^{n-1} + \ell_1^n(t)\mathcal{R}^n U^n$ ,  $t \in I_n$ . Thus (2.6), (2.19) yield

$$(3.11) \quad \begin{aligned} \langle (-\alpha \Delta + g(t))\omega(t), \phi \rangle &= \alpha \langle \Theta(t), \phi \rangle + \alpha \ell_0^n(t) \langle (I^n - I)\Delta^{n-1}U^{n-1}, \phi \rangle + \langle (gU)(t), \phi \rangle \\ &\quad + \langle (g(t) - \bar{g}_n)[\ell_0^n(t)(\mathcal{R}^{n-1} - I)U^{n-1} + \ell_1^n(t)(\mathcal{R}^n - I)U^n], \phi \rangle. \end{aligned}$$

Similarly, in view of (2.26), we obtain

$$(3.12) \quad \begin{aligned} \langle (-\alpha \Delta + g(t))\sigma(t), \phi \rangle &= \frac{1}{2}(t_n - t)(t - t_{n-1}) \times \\ &\quad \langle (-\alpha \Delta^n + g(t))\bar{\partial}W^{n-\frac{1}{2}} + (g(t) - \bar{g}_n)(\mathcal{R}^n - I)\bar{\partial}W^{n-\frac{1}{2}}, \phi \rangle. \end{aligned}$$

Combining (3.10), (3.4) with (3.11), (3.12) and using (2.20) we arrive at (3.5).  $\square$

Next, we prove the following auxiliary lemma.

**Lemma 3.1.** *The residual  $R_1$  in (3.6) can be rewritten as*

$$(3.13) \quad \begin{aligned} R_1(t) &= (t - t_{n-\frac{1}{2}})(\mathcal{R}^n - I)\bar{\partial}W^{n-\frac{1}{2}} - \frac{(\mathcal{R}^n - I)U^n - (\mathcal{R}^{n-1} - I)U^{n-1}}{k_n} \\ &\quad + (I - I^n)(i\alpha \ell_0^n(t)\Delta^{n-1}U^{n-1} + \frac{U^{n-1}}{k_n}), \quad t \in I_n. \end{aligned}$$

*Proof.* We just note, using the method in the form (2.22), that

$$(\mathcal{R}^n - I)W(t_{n-\frac{1}{2}}) - \frac{\mathcal{R}^n I^n U^{n-1} - \mathcal{R}^{n-1}U^{n-1}}{k_n} = \frac{(I - \mathcal{R}^n)U^n - (I - \mathcal{R}^{n-1})U^{n-1}}{k_n} + (I - I^n)\frac{U^{n-1}}{k_n}.$$

The result follows in light of (2.23), because  $\partial_t W(t) = \bar{\partial}W^{n-\frac{1}{2}}$  for  $t \in I_n$ .  $\square$

Proposition 3.3 and Lemma 3.1 together with energy methods, lead to the following a posteriori estimation in the  $L^\infty(L^2)$ -norm for the main error  $\hat{\rho}$ .

**Proposition 3.4** (estimation of the main error). *Let  $p_n := \sup_{\Omega \times I_n} |g(x, t) - \bar{g}_n|$ ,  $1 \leq n \leq N$ . Then, for the main error  $\hat{\rho} = u - \hat{U}$  and  $1 \leq m \leq N$ , it holds that*

$$(3.14) \quad \max_{0 \leq t \leq t_m} \|\hat{\rho}(t)\| \leq \|u_0 - \mathcal{R}^0 U^0\| + \mathcal{E}_m^{\text{T},1} + C(\mathcal{E}_m^{\text{S},1} + \mathcal{E}_m^{\text{S},2}) + \widehat{C}\mathcal{E}_m^{\text{S},3} + \mathcal{E}_m^{\text{C}} + \mathcal{E}_m^{\text{D}},$$

where the time estimator  $\mathcal{E}_m^{\text{T},1}$  is given by

$$(3.15) \quad \mathcal{E}_m^{\text{T},1} := \sum_{n=1}^m \int_{t_{n-1}}^{t_n} \frac{(t_n - t)(t - t_{n-1})}{2} \|(-\alpha \Delta^n + g(t))\bar{\partial}W^{n-\frac{1}{2}}\| dt + C \sum_{n=1}^m \frac{k_n^3}{24} p_n \eta_{\mathbb{V}^n}(\bar{\partial}W^{n-\frac{1}{2}}),$$

the space estimators  $\mathcal{E}_m^{\text{S},j}$ ,  $1 \leq j \leq 3$ , are given by

$$(3.16) \quad \begin{aligned} \mathcal{E}_m^{\text{S},1} &:= \sum_{n=1}^m \frac{k_n^2}{4} \eta_{\mathbb{V}^n}(\bar{\partial}W^{n-\frac{1}{2}}), & \mathcal{E}_m^{\text{S},2} &:= \sum_{n=1}^m \frac{k_n}{2} p_n (\eta_{\mathbb{V}^{n-1}}(U^{n-1}) + \eta_{\mathbb{V}^n}(U^n)), \\ \text{and } \mathcal{E}_m^{\text{S},3} &:= \sum_{n=1}^m k_n \eta_{\widehat{\mathbb{V}}^n} \left( \frac{U^n}{k_n}, \frac{U^{n-1}}{k_n} \right), \end{aligned}$$

and the coarsening and data estimators  $\mathcal{E}_m^{\text{C}}$  and  $\mathcal{E}_m^{\text{D}}$  are

$$(3.17) \quad \mathcal{E}_m^{\text{C}} := \sum_{n=1}^m \int_{t_{n-1}}^{t_n} \|(I - I^n) \left( \frac{U^{n-1}}{k_n} + i\alpha \ell_0^n(t)\Delta^{n-1}U^{n-1} \right)\| dt,$$

and

$$(3.18) \quad \mathcal{E}_m^{\text{D}} := \sum_{n=1}^m \int_{t_{n-1}}^{t_n} \left[ \|\mathcal{P}^n G_U(t) - (gU)(t)\| + \|f(t) - \mathcal{P}^n F(t)\| \right] dt,$$

respectively.

*Proof.* Setting  $\phi = \hat{\rho}$  in (3.5) and taking real parts yields

$$\frac{1}{2} \frac{d}{dt} \|\hat{\rho}(t)\|^2 = \operatorname{Re} \left\langle \sum_{j=1}^4 R_j(t), \hat{\rho}(t) \right\rangle \leq \sum_{j=1}^4 \|R_j(t)\| \|\hat{\rho}(t)\|, \quad t \in I_n,$$

or,

$$(3.19) \quad \max_{0 \leq t \leq t_m} \|\hat{\rho}(t)\| \leq \|\hat{\rho}(0)\| + \sum_{j=1}^4 \int_0^{t_m} \|R_j(t)\| dt.$$

Then, it is easily seen that

$$(3.20) \quad \int_0^{t_m} \|R_1(t)\| dt \leq \mathcal{E}_m^{S,1} + \mathcal{E}_m^{S,3} + \mathcal{E}_m^C;$$

cf. (3.13), and

$$(3.21) \quad \int_0^{t_m} \|R_2(t)\| dt \leq \mathcal{E}_m^{T,1}, \quad \int_0^{t_m} \|R_3(t)\| dt \leq \mathcal{E}_m^{S,2}, \quad \int_0^{t_m} \|R_4(t)\| dt \leq \mathcal{E}_m^D;$$

cf. (3.7)–(3.9). Going back to (3.19) and plugging in (3.20)–(3.21) we readily obtain (3.14).  $\square$

**Remark 3.1** (optimal order of the estimators in (3.14)). It is clear that the space estimators  $\mathcal{E}_m^{S,j}$ ,  $1 \leq j \leq 3$ , are expected to be of optimal order of accuracy in space. In fact, estimator  $\mathcal{E}_m^{S,1}$  is expected to be of optimal order in space and of order one in time, i.e., it is a superconvergent term. As far as the first part of the time estimator  $\mathcal{E}_m^{T,1}$  is concerned, we note that

$$\int_{t_{n-1}}^{t_n} \frac{(t_n - t)(t - t_{n-1})}{2} \|(-\alpha \Delta^n + g(t)) \bar{\partial} W^{n-\frac{1}{2}}\| dt \leq \frac{k_n^3}{12} \sup_{t \in I_n} \|(-\alpha \Delta^n + g(t)) \bar{\partial} W^{n-\frac{1}{2}}\|.$$

So, it is expected to be of optimal order of accuracy in time. Numerically, this term can be computed by invoking a quadrature in time, which is at least second order accurate (i.e., at least as accurate as the accuracy of the discretization method in time). The second part of  $\mathcal{E}_m^{T,1}$  is expected to be of optimal order in both time and space. On the other hand, note that estimator  $\mathcal{E}_m^C$  is not identically zero, only during the coarsening procedure. Finally, for the estimators related to the data of the problem we have  $\|u_0 - \mathcal{R}^0 U^0\| \leq \|u_0 - U^0\| + C \eta_{\mathbb{V}^0}(U^0)$  and  $\|\mathcal{P}^n G_U(t) - (gU)(t)\| \leq \|(\mathbf{I} - \mathcal{P}^n) G_U(t)\| + \|(G_U - gU)(t)\|$ . The term  $\|f(t) - \mathcal{P}^n F(t)\|$  is handled similarly. Thus, it is straightforward to see that  $\mathcal{E}_m^D$  can be split into optimal order estimators in time and space, while  $\|u_0 - \mathcal{R}^0 U^0\|$  is easily estimated a posteriori via optimal order estimators in space.

**Remark 3.2** (the constants  $p_n$ ). For the constants  $p_n$  we note that  $p_n \leq p_{n,1} + p_{n,2}$  with  $p_{n,1} := \sup_{\Omega \times I_n} |g(x, t) - g(x, t_{n-\frac{1}{2}})|$  and  $p_{n,2} = \frac{1}{2} [\sup_{x \in \Omega} |g(x, t_{n-\frac{1}{2}})| - \inf_{x \in \Omega} |g(x, t_{n-\frac{1}{2}})|]$ . Therefore,  $p_{n,1} = \mathcal{O}(k_n)$ , while  $p_{n,2}$  is relatively small, provided that  $g$  does not change much, with respect to the spatial variable. More precisely,  $p_{n,2} \equiv 0$  when  $g$  is constant in space, while the estimators that are multiplied by  $p_n$  in (3.14) vanish for constant potentials. This particular behavior of the estimators is natural from physical point of view.

We conclude with the main theorem of the paper.

**Theorem 3.1** (a posteriori error estimate in the  $L^\infty(L^2)$ -norm). *Let  $u$  be the exact solution of (1.1) and let  $U$  be the continuous approximation (2.15) of  $u$  related to the modified Crank-Nicolson-Galerkin method (2.4). Then, the following estimate is valid for  $1 \leq m \leq N$ :*

$$(3.22) \quad \max_{0 \leq t \leq t_m} \|(u - U)(t)\| \leq \|u_0 - \mathcal{R}^0 U^0\| + \mathcal{E}_m^{T,0} + \mathcal{E}_m^{T,1} + C \sum_{j=0}^2 \mathcal{E}_m^{S,j} + \widehat{C} \mathcal{E}_m^{S,3} + \mathcal{E}_m^C + \mathcal{E}_m^D,$$

where  $\mathcal{E}_m^{T,1}$ ,  $\mathcal{E}_m^{S,j}$ ,  $1 \leq j \leq 3$ ,  $\mathcal{E}_m^C$ ,  $\mathcal{E}_m^D$  are given by (3.15), (3.16), (3.17) and (3.18) and  $\mathcal{E}_m^{T,0}$ ,  $\mathcal{E}_m^{S,0}$  are as in (3.1) and (3.2), respectively.

*Proof.* We write  $u - U = \hat{\rho} + \sigma + \epsilon$ , whence, for  $1 \leq m \leq N$ ,

$$\max_{0 \leq t \leq t_m} \|(u - U)(t)\| \leq \max_{0 \leq t \leq t_m} \|\hat{\rho}(t)\| + \max_{0 \leq t \leq t_m} \|\sigma(t)\| + \max_{0 \leq t \leq t_m} \|\epsilon(t)\|.$$

Estimate (3.22) is now an immediate consequence of Propositions 3.2, 3.1 and 3.4.  $\square$

## 4. NUMERICAL EXPERIMENTS: UNIFORM PARTITION

In this section, we perform various numerical experiments for the one-dimensional linear semiclassical Schrödinger equation:

$$(4.1) \quad \partial_t u - i \frac{\varepsilon}{2} \partial_{xx} u + \frac{i}{\varepsilon} V(x, t) u = 0 \quad \text{in } (a, b) \times (0, T],$$

using uniform partitions. Our experiments, not only illustrate and complement our theoretical results, but also give important information in several other interesting aspects, like the behavior of the estimators with respect to the parameter  $\varepsilon$ . At the moment, the particular behavior can only be proven formally; cf. Subsection 4.2. In all of the numerical experiments, the initial data is of the well known semiclassical WKB form:

$$(4.2) \quad u_0(x) = \sqrt{n_0(x)} e^{i \frac{S_0(x)}{\varepsilon}}.$$

In (4.2),  $n_0$  and  $S_0$  are real and smooth functions on  $[a, b]$ . In addition,  $n_0$  is positive on  $(a, b)$  and vanishes (numerically) at the endpoints  $a$  and  $b$ .

The modified Galerkin-Crank-Nicolson method (2.4) and the corresponding a posteriori error estimators for problem (4.1)-(4.2) with homogeneous Dirichlet boundary conditions, were implemented in a double precision C-code, using B-splines of degree  $r$ ,  $r \in \mathbb{N}$ , as a basis for the finite element space  $\mathbb{V}^n$ ,  $0 \leq n \leq N$ . The involved projections  $\mathbb{H}^n$  and  $\mathcal{P}^n$  in (2.4) are taken to be the  $L^2$ -projection onto  $\mathbb{V}^n$ .

In what follows, we present some characteristic examples that allow us to verify the correct order of convergence of the estimators in time and space, and their dependence on the Planck constant  $\varepsilon$ . We also report on the relation between the time and space mesh sizes with respect to  $\varepsilon$  in order to have convergence.

**4.1. EOC of the estimators.** We proceed by studying two different cases. The first one concerns time-independent potentials, while in the second one we consider a time-dependent potential.

EXPERIMENT 1 (Time-independent potentials). Here, we consider three well-known types of potential: a constant potential, a harmonic oscillator and a double-well potential ([31, 14, 25]). In all three examples, the Planck constant is taken to be of order 1. More precisely, we study the following cases:

- a.  $V(x) = 100$ ,  $\sqrt{n_0(x)} = e^{-\frac{25}{2}x^2}$ ,  $S_0(x) = \frac{x^2}{2}$ , and  $\varepsilon = 1$ ;
- b.  $V(x) = \frac{x^2}{2}$ ,  $\sqrt{n_0(x)} = e^{-25(x-0.5)^2}$ ,  $S_0(x) = 1 + x$ , and  $\varepsilon = 0.5$ ;
- c.  $V(x) = (x^2 - 0.25)^2 = x^4 - \frac{1}{2}x^2 + \frac{1}{16}$ ,  $\sqrt{n_0(x)} = e^{-\frac{25}{2}x^2}$ ,  $S_0(x) = -\frac{1}{5} \ln \left( e^{5(x-0.5)} + e^{-5(x-0.5)} \right)$ , and  $\varepsilon = 0.25$ .

All computations are performed in  $[a, b] \times [0, T] = [-2, 2] \times [0, 1]$ . Our purpose is to compute the *experimental order of convergence* (EOC) of the a posteriori error estimators at the final time  $T = 1$ . For this, we consider uniform partitions in both time and space. If we denote by  $r$  the degree of B-splines used for the discretization in space, then in each implementation, the relation between the mesh size  $h$  and the time step  $k$  is taken to be

$$(4.3) \quad h \approx k^{\frac{2}{r+1}}$$

with equality, whenever possible. We also denote by  $M = \frac{b-a}{h}$ . Then, for each space estimator  $\mathcal{E}_N^{S,j}$ ,  $0 \leq j \leq 3$ , the EOC is computed as

$$(4.4) \quad \text{EOC} := \frac{\log \left( \mathcal{E}_N^{S,j}(\ell) / \mathcal{E}_N^{S,j}(\ell+1) \right)}{\log \left( M(\ell+1) / M(\ell) \right)},$$

where  $\mathcal{E}_N^{S,j}(\ell)$  and  $\mathcal{E}_N^{S,j}(\ell+1)$  denote the value of the estimators in two consecutive implementations with mesh sizes  $h(\ell) = \frac{b-a}{M(\ell)}$  and  $h(\ell+1) = \frac{b-a}{M(\ell+1)}$ , respectively. Note that  $\mathcal{E}_N^{S,1}$  is expected to be of optimal order in space and of order 1 in time, i.e., it is a superconvergent term. Therefore, the EOC we expect to observe is  $h^{r+1} \cdot h^{\frac{r+1}{2}} = h^{\frac{3}{2}(r+1)}$ , due to (4.3) and (4.4). Similarly, for the time estimators  $\mathcal{E}_N^{T,j}$ ,  $0 \leq j \leq 1$ , the EOC is computed as

$$(4.5) \quad \text{EOC} := \frac{\log \left( \mathcal{E}_N^{T,j}(\ell) / \mathcal{E}_N^{T,j}(\ell+1) \right)}{\log \left( k(\ell) / k(\ell+1) \right)}.$$

We are also interested in computing the *effectivity index*, defined as the ratio between the total a posteriori error estimator and the corresponding norm of the exact error. Since we do not have at our disposal the exact solution for the three examples, we compute a reference solution  $u_{\text{ref}}$  instead, by taking very fine mesh and

time step. In particular, we take as  $k_{\text{ref}}^{-1} = 40960$ , while in space we discretize by B-splines of degree 5 and take as  $h_{\text{ref}}^{-1} = 120$ . Then, the reference error is defined as  $\text{Eref} := \max_{0 \leq n \leq N} \|u_{\text{ref}}(t_n) - U^n\|$ . In addition, we define

$$\mathcal{E}_N^{\text{total}} := \|u_0 - U^0\| + \eta_{\text{vo}}(U^0) + \mathcal{E}_N^{\text{T},0} + \mathcal{E}_N^{\text{T},1} + \sum_{j=0}^3 \mathcal{E}_N^{\text{S},j} + \mathcal{E}_N^{\text{D}},$$

and we compute the effectivity index  $ei$  as  $ei := \mathcal{E}_N^{\text{total}}/\text{Eref}$ . Note that for uniform partitions, the coarsening estimator  $\mathcal{E}_N^{\text{C}}$  is identically zero. Our findings are reported in Tables 1–6.

In the case of constant potential  $V(x) = 100$ , we discretize in space by linear B-splines. We recall that in this case  $\mathcal{E}_N^{\text{S},2}$  is identically zero and does not appear in Table 1. As we see in Tables 1, 2, all estimators decrease with the correct order. We observe that the total error is mainly due to the time estimator  $\mathcal{E}_N^{\text{T},1}$ ,

$M$	$\mathcal{E}_N^{\text{S},0}$	EOC	$\mathcal{E}_N^{\text{S},1}$	EOC	$\mathcal{E}_N^{\text{S},3}$	EOC
640	5.0445e-04	–	1.3289e-02	–	6.1493e-02	–
1280	1.2609e-04	2.0003	1.7796e-03	2.9006	1.6361e-02	1.9102
2560	3.1522e-05	2.0000	2.2677e-04	2.9722	4.1610e-03	1.9753
5120	7.8804e-06	2.0000	2.8488e-05	2.9928	1.0448e-03	1.9937
10240	1.9701e-06	2.0000	3.5665e-06	2.9978	2.6150e-04	1.9983

TABLE 1. Space estimators  $\mathcal{E}_N^{\text{S},j}$ ,  $j = 0, 1, 3$ , and EOC for Experiment 1a.

$k^{-1}$	$\mathcal{E}_N^{\text{T},0}$	EOC	$\mathcal{E}_N^{\text{T},1}$	EOC	Eref	$\mathcal{E}_N^{\text{total}}$	$ei$
160	3.1810e-02	–	2.3471	–	1.1329	2.4547	2.1668
320	8.2836e-03	1.9411	6.1356e-01	1.9356	5.4529e-01	6.4024e-01	1.1741
640	2.0935e-03	1.9843	1.5524e-01	1.9827	1.5026e-01	1.6178e-01	1.0767
1280	5.2481e-04	1.9960	3.8928e-02	1.9956	3.8853e-02	4.0541e-02	1.0434
2560	1.3129e-04	2.0090	9.7395e-03	1.9989	9.6973e-03	1.0140e-02	1.0456

TABLE 2. Time estimators  $\mathcal{E}_N^{\text{T},j}$ ,  $j = 0, 1$ , and EOC, total estimator  $\mathcal{E}_N^{\text{total}}$ , reference error Eref, and effectivity index  $ei$  for Experiment 1a.

while the effectivity index is around 1.04, i.e., the total estimator  $\mathcal{E}_N^{\text{total}}$  is very close to the reference error. However constant potentials are the simplest; actually, from physical point of view, having a constant potential is like having no potential at all.

In Tables 3, 4 the results for the harmonic oscillator (1b) are presented. We use quadratic B-splines for the discretization in space. The correct order of convergence is observed for all estimators. The dominant estimator for the harmonic oscillator is  $\mathcal{E}_N^{\text{S},3}$ , while the effectivity index tends asymptotically to the constant value 4.5.

$M$	$\mathcal{E}_N^{\text{S},0}$	EOC	$\mathcal{E}_N^{\text{S},1}$	EOC	$\mathcal{E}_N^{\text{S},2}$	EOC	$\mathcal{E}_N^{\text{S},3}$	EOC
75	1.3042e-02	–	1.5619e-01	–	2.4735e-02	–	6.3657e-01	–
120	3.1817e-03	3.0016	2.1398e-02	4.2293	6.0463e-03	2.9974	1.6747e-01	2.8410
185	8.6805e-04	3.0008	3.0282e-03	4.5172	1.6509e-03	2.9989	4.6712e-02	2.9497
295	2.1405e-04	3.0004	3.7707e-04	4.4646	4.0737e-04	2.9989	1.1585e-02	2.9881
470	5.2927e-05	3.0000	4.6730e-05	4.4831	1.0077e-04	2.9992	2.8684e-03	2.9972
750	1.3025e-05	3.0000	5.7532e-06	4.4820	2.4807e-05	2.9993	7.0610e-04	2.9994

TABLE 3. Space estimators  $\mathcal{E}_N^{\text{S},j}$ ,  $0 \leq j \leq 3$ , and EOC for Experiment 1b.

$k^{-1}$	$\mathcal{E}_N^{T,0}$	EOC	$\mathcal{E}_N^{T,1}$	EOC	Eref	$\mathcal{E}_N^{\text{total}}$	$ei$
80	5.7695e-03	–	2.0831e-01	–	1.0412e-01	1.0596	10.1767
160	1.3258e-03	2.1216	5.6917e-02	1.8718	4.3944e-02	2.6041e-01	5.9259
320	3.2430e-04	2.0314	1.4648e-02	1.9581	1.3199e-02	6.8543e-02	5.1930
640	8.0510e-05	2.0101	3.6910e-03	1.9886	3.5667e-03	1.6784e-02	4.7057
1280	2.0093e-05	2.0025	9.2463e-04	1.9971	9.2127e-04	4.1723 e-03	4.5289
2560	5.0210e-06	2.0006	2.3128e-04	1.9992	2.3004e-04	1.0513e-03	4.5701

TABLE 4. Time estimators  $\mathcal{E}_N^{T,j}$ ,  $j = 0, 1$ , and EOC, total estimator  $\mathcal{E}_N^{\text{total}}$ , reference error Eref, and effectivity index  $ei$  for Experiment 1b.

$M$	$\mathcal{E}_N^{S,0}$	EOC	$\mathcal{E}_N^{S,1}$	EOC	$\mathcal{E}_N^{S,2}$	EOC	$\mathcal{E}_N^{S,3}$	EOC
35	2.2902e-02	–	3.0041e-02	–	3.7853e-01	–	3.0978e-01	–
50	5.1709e-03	4.1724	3.5161e-03	6.0145	8.7250e-02	4.1144	7.1970e-02	4.0923
70	1.2925e-03	4.1206	4.3823e-04	6.1888	2.2013e-02	4.0929	1.8017e-02	4.1160
100	3.0294e-04	4.0676	5.0898e-05	6.0361	5.1836e-03	4.0545	4.2076e-03	4.0777
145	6.7657e-05	4.0345	5.6498e-06	5.9161	1.1609e-03	4.0270	9.3722e-04	4.0416
200	1.8587e-05	4.0176	7.7427e-07	6.1802	3.1941e-04	4.0129	2.5721e-04	4.0208

TABLE 5. Space estimators  $\mathcal{E}_N^{S,j}$ ,  $0 \leq j \leq 3$ , and EOC for Experiment 1c.

$k^{-1}$	$\mathcal{E}_N^{T,0}$	EOC	$\mathcal{E}_N^{T,1}$	EOC	Eref	$\mathcal{E}_N^{\text{total}}$	$ei$
80	1.2555e-03	–	1.6010e-02	–	1.2414e-02	7.8510e-01	63.2431
160	2.5490e-04	2.3003	3.6767e-03	2.1225	3.4441e-03	1.7773e-01	51.6042
320	6.0463e-05	2.0758	9.0229e-04	2.0267	9.7835e-04	4.4277e-02	45.2568
640	1.4911e-05	2.0197	2.2452e-04	2.0067	2.1739e-04	1.0409e-02	47.8817
1280	3.7157e-06	2.0047	5.6068e-05	2.0016	5.5890e-05	2.3622e-03	42.2652
2560	9.2832e-07	2.0009	1.4014e-05	2.0003	1.3946e-05	6.6728e-04	47.8474

TABLE 6. Time estimators  $\mathcal{E}_N^{T,j}$ ,  $j = 0, 1$ , and EOC, total estimator  $\mathcal{E}_N^{\text{total}}$ , reference error Eref, and effectivity index  $ei$  for Experiment 1c.

Finally, for the double-well potential (1c), we discretize in space by cubic B-splines. The results are listed in Tables 5, 6. For this example, the effectivity index seems to be asymptotically constant (around 47.8), but it is certainly larger compared to the previous two examples. This is maybe an indicator that the presented analysis can be improved, in order to end-up with better effectivity indices. Effectivity indices of this size were also observed in experiments for the two-dimensional heat equation, for backward Euler finite element schemes ([21]) and for the corresponding to (2.4) method ([6]).

EXPERIMENT 2 (A time-dependent potential). In the second experiment we consider the time-dependent potential  $V(x, t) = (1+t)^2 \frac{x^2}{2}$ . Such potentials were studied for example in [22, 8]. In order to have an example where we can evaluate the exact error, instead of solving numerically problem (4.1)–(4.2) with zero Dirichlet boundary conditions, we replace (4.1) by

$$(4.6) \quad \partial_t u - \frac{i}{2} \partial_{xx} u + iV(x, t)u = f(x, t)$$

(for this experiment,  $\varepsilon = 1$ ). We consider as exact solution  $u(x, t) = e^{-25(x-t)^2} e^{i(1+t)(1+x)}$  and we calculate  $f$  through (4.6).

We take again  $[a, b] \times [0, T] = [-2, 2] \times [0, 1]$  and we perform the same computations as in Experiment 1. In space, we discretize by quadratic B-splines. The numerical results are reported in Tables 7, 8. The correct order of convergence is observed for the estimators. The effectivity index tends asymptotically to a

$M$	$\mathcal{E}_N^{S,0}$	EOC	$\mathcal{E}_N^{S,1}$	EOC	$\mathcal{E}_N^{S,2}$	EOC	$\mathcal{E}_N^{S,3}$	EOC
75	1.3090e-02	–	7.2318e-03	–	2.8864e-02	–	1.4480e-01	–
120	3.1864e-03	3.0063	7.9989e-04	4.6846	7.0052e-03	3.0126	3.5234e-02	3.0071
185	8.6868e-04	3.0025	1.0649e-04	4.6583	1.9068e-03	3.0061	9.6015e-03	3.0035
295	2.1412e-04	3.0012	1.3072e-05	4.5036	4.6970e-04	3.0026	2.3665e-03	3.0069
470	5.2935e-05	3.0004	1.6152e-06	4.4895	1.1608e-04	3.0012	5.8502e-04	3.0005
750	1.3026e-05	3.0002	1.9878e-07	4.4826	2.8560e-05	3.0005	1.4396e-04	3.0002
1190	3.2610e-06	3.0000	2.4920e-08	4.4982	7.1492e-06	3.0002	3.6039e-05	3.0000
1885	8.2045e-07	3.0000	3.7518e-09	4.1164	1.7986e-06	3.0001	9.0671e-06	3.0001

TABLE 7. Space estimators  $\mathcal{E}_N^{S,j}$ ,  $0 \leq j \leq 3$ , and EOC for Experiment 2.

$k^{-1}$	$\mathcal{E}_N^{T,0}$	EOC	$\mathcal{E}_N^{T,1}$	EOC	Eex	$\mathcal{E}_N^{\text{total}}$	$ei$
80	6.9252e-04	–	3.3241e-02	–	6.6552e-04	2.6595e-01	399.612
160	1.6443e-04	2.0744	7.7801e-03	2.0951	1.6474e-04	6.2511e-02	379.4525
320	4.0878e-05	2.0081	1.9170e-03	2.0209	4.1787e-05	1.6624e-02	397.8271
640	1.0204e-05	2.0022	4.7815e-04	2.0033	1.0658e-05	4.0799e-03	382.8016
1280	2.5513e-06	1.9998	1.1953e-04	2.0000	2.6883 e-06	1.0073e -03	374.6978
2560	6.3801e-07	1.9996	2.9888e-05	1.9997	6.7413e-07	2.4807e-04	367.9854
5120	1.5988e-07	1.9968	7.4898e-06	1.9966	1.6935e-07	6.2075e-05	366.5486
10240	3.9973e-08	2.0000	1.8728e-06	1.9997	4.2433e-08	1.5602e-05	367.6855

TABLE 8. Time estimators  $\mathcal{E}_N^{T,j}$ ,  $j = 0, 1$ , and EOC, total estimator  $\mathcal{E}_N^{\text{total}}$ , exact error Eex, and effectivity index  $ei$  for Experiment 2.

constant value, which is around 368, which is a strong indication that there maybe room for improvement of the analysis. We point out though, that no a posteriori error bounds of optimal order exist in the literature for time-dependent potentials and any numerical method. It is the first time that a complete a posteriori error analysis is provided and numerically verified for operators of the form  $i(-\Delta + V(x, t))$ .

**4.2.  $\varepsilon$ -sensitivity of the estimators.** In the case of WKB initial data for the problem (4.1)-(4.2) one can show that

$$\sup_{0 \leq t \leq T} \left\| \frac{\partial^m u}{\partial t^m}(t) \right\| = \mathcal{O}\left(\frac{1}{\varepsilon^m}\right) \quad \text{and} \quad \sup_{0 \leq t \leq T} \left\| \frac{\partial^m u}{\partial x^m}(t) \right\| = \mathcal{O}\left(\frac{1}{\varepsilon^m}\right), \quad m \in \mathbb{N}_0,$$

provided  $n_0$ ,  $S_0$  and  $V$  are regular enough; [2]. In that respect, and assuming that  $U^n$ ,  $0 \leq n \leq N$ , are reasonably good approximations to  $u$  at the nodes  $t_n$ , we expect the following behavior of the a posteriori error estimators with respect to the parameter  $\varepsilon$ :

$$(4.7) \quad \mathcal{E}_N^{S,0} = \mathcal{O}\left(\frac{h^{r+1}}{\varepsilon^{r+1}}\right), \quad \mathcal{E}_N^{S,1} = \mathcal{O}\left(\frac{h^{r+1} k}{\varepsilon^{r+2} \varepsilon}\right), \quad \mathcal{E}_N^{S,2} = \mathcal{O}\left(\frac{h^{r+1}}{\varepsilon^{r+2}}\right), \quad \mathcal{E}_N^{S,3} = \mathcal{O}\left(\frac{h^{r+1}}{\varepsilon^{r+2}}\right),$$

$$(4.8) \quad \mathcal{E}_N^{T,0} = \mathcal{O}\left(\frac{k^2}{\varepsilon^2} \left(1 + \frac{h^{r+1}}{\varepsilon^{r+1}}\right)\right), \quad \mathcal{E}_N^{T,1} = \mathcal{O}\left(\frac{k^2}{\varepsilon^3} \left(1 + \frac{h^{r+1}}{\varepsilon^{r+2}}\right)\right).$$

Relations (4.7)–(4.8) give us an idea on how we have to choose the time and space steps so that the estimators converge. The suggested choice seems to be restrictive; however it is the expected one. Indeed the a priori error analysis for CNFE schemes gives that

$$(4.9) \quad \max_{0 \leq n \leq N} \|u(t_n) - U^n\| = \mathcal{O}\left(\frac{h^{r+1}}{\varepsilon^{r+2}} + \frac{k^2}{\varepsilon^3}\right),$$

cf. [2], and naturally, conditions (4.7)–(4.8) were not expected to be more relaxed. Next, we verify numerically (4.7)–(4.8). To this end, we consider  $\sqrt{n_0(x)} = e^{-25(x-0.5)^2}$ ,  $S_0(x) = -\frac{1}{5} \ln\left(e^{5(x-0.5)} + e^{-5(x-0.5)}\right)$ , and the constant potential  $V(x) = 10$ . We solve numerically problem (4.1)–(4.2) in  $(a, b) \times (0, T] = (-1, 2) \times (0, 0.54]$ , for  $\varepsilon = 0.005$  and  $\varepsilon = 0.001$ , using B-splines of degree 1 or 3. Since the potential is taken to be constant, estimator  $\mathcal{E}_N^{S,2}$  is identically zero. The particular example has been considered earlier in [2] (see also [27]) and it is interesting because caustics are formed before the final time  $T = 0.54$ .

First, we consider the case  $\varepsilon = 0.005$ . We discretize by B-splines of degree 1 and we consider uniform partitions in both time and space with  $k = h$ . The behavior of the space and time a posteriori error estimators are reported in Table 9. As (4.7) suggests, estimator  $\mathcal{E}_N^{S,1}$  has the expected behavior for  $k = h \leq 5 \times 10^{-4}$ ,

$k = h$	$\mathcal{E}_N^{S,0}$	$\mathcal{E}_N^{S,1}$	$\mathcal{E}_N^{S,3}$	$\mathcal{E}_N^{T,0}$	$\mathcal{E}_N^{T,1}$
$10^{-2}$	5.9846e-01	3.3162e+02	6.4332e+01	5.5855	1.8291e+03
$10^{-3}$	5.1220e-03	2.0283	3.9587	1.8122e-01	1.3029e+02
$5 \times 10^{-4}$	1.2789e-03	3.2267e-01	1.2595	5.7015e-02	4.1315e+01
$10^{-4}$	5.1137e-05	2.8842e-03	5.6296e-02	2.5351e-03	1.8417
$5 \times 10^{-5}$	1.2784e-05	3.6194e-04	1.4128e-02	6.3615e-04	4.6218e-01
$10^{-5}$	5.1136e-07	3.2460e-06	5.6582e-04	2.5476e-05	1.8510e-02

TABLE 9. Space estimators  $\mathcal{E}_N^{S,j}$ ,  $j = 0, 1, 3$ , and time estimators  $\mathcal{E}_N^{T,j}$ ,  $j = 0, 1$ , for  $\varepsilon = 0.005$ .

while  $\mathcal{E}_N^{S,3}$  for  $h \leq 10^{-4}$ . Similar results, verifying (4.8), are observed for the time estimators  $\mathcal{E}_N^{T,0}$  and  $\mathcal{E}_N^{T,1}$ . In particular, note that for  $k \geq 10^{-4}$ ,  $\mathcal{E}_N^{T,1}$  is not reasonable, something we expect, provided that (4.8) is true and  $\varepsilon = 0.005$ . Note however, that estimator  $\mathcal{E}_N^{S,0}$  behaves better than expected, since for  $h = 10^{-2}$  it already decays with optimal order.

Next, we consider the case  $\varepsilon = 0.001$ . We discretize in space by cubic B-splines. To verify numerically (4.7), we take constant time step,  $k = 5 \times 10^{-3}$  so that  $\frac{k}{\varepsilon} = \mathcal{O}(1)$ , and thus be able to see only the effect of the space discretization with respect to  $\varepsilon$  for  $\mathcal{E}_N^{S,1}$ . As before, in Table 10, the stated relation (4.7) between  $h$  and  $\varepsilon$  is observed for  $\mathcal{E}_N^{S,1}$  and  $\mathcal{E}_N^{S,3}$ . We also verify the corresponding relation between  $h$  and  $\varepsilon$  in (4.7) for  $\mathcal{E}_N^{S,0}$ . Indeed, despite the fact that  $\mathcal{E}_N^{S,0}$  is small, even for  $M = 600$  ( $h = 5 \times 10^{-3}$ ), it does not decay with optimal order. The correct behavior is initiated for  $M = 1500$  ( $h = 2 \times 10^{-3}$ ), and verified for  $M = 3000$  ( $h = 10^{-3}$ ). For the time estimators, (4.8) is verified with constant mesh size  $h = 5 \times 10^{-4}$  ( $M = 6000$ ). Our choice of  $h$  is so that  $\frac{h^4}{\varepsilon^5}$  is controlled, and allow us to exploit the behavior of  $k$  with respect to  $\varepsilon$ . Our findings are shown in Table 10.

$M$	$\mathcal{E}_N^{S,0}$	$\mathcal{E}_N^{S,1}$	$\mathcal{E}_N^{S,3}$	$k$	$\mathcal{E}_N^{T,0}$	$\mathcal{E}_N^{T,1}$
600	3.6649e-01	2.4658e+02	1.9454e+03	$10^{-3}$	1.2389	4.4981e+03
1500	4.6616e-02	3.2401e+01	2.5136e+02	$5 \times 10^{-4}$	5.8702e-01	2.1314e+03
3000	2.6006e-03	1.8065	1.4019e+01	$10^{-4}$	5.6881e-02	2.0655e+02
4500	4.9896e-04	3.4653e-01	2.6894	$5 \times 10^{-5}$	1.5444e-02	5.6083e+01
6000	1.5618e-04	1.0846e-01	8.4179e-01	$10^{-5}$	6.3630e-04	2.3107
7500	6.3646e-05	4.4198e-02	3.4304e-01	$5 \times 10^{-6}$	1.5923e-04	5.7822e-01
9000	3.0608e-05	2.1254e-02	1.6497e-01	$2.5 \times 10^{-6}$	3.9816e-05	1.4459e-01

TABLE 10. Space estimators  $\mathcal{E}_N^{S,j}$ ,  $j = 0, 1, 3$ , with  $k = 5 \times 10^{-5}$ , and time estimators  $\mathcal{E}_N^{T,j}$ ,  $j = 0, 1$ , with  $M = 6000$ , for  $\varepsilon = 0.001$ .

## 5. NUMERICAL EXPERIMENTS: ADAPTIVITY

In this section, we adjust and further develop a time-space adaptive algorithm for linear Schrödinger equations, using the a posteriori error estimators derived earlier. Our goal is to study numerically the behavior of the estimators under this adaptive algorithm, and investigate the benefits, in terms of computational cost and accuracy, of time-space adaptivity.

To this end, we consider, as in the previous section, the one-dimensional linear Schrödinger equation in the semiclassical regime, cf. (4.1), along with the WKB initial condition (4.2). The presented numerical experiments indicate that adaptivity through the a posteriori error bounds is indeed advantageous, especially for relatively small values of the Planck constant  $\varepsilon$ , for both time-independent and time-dependent potentials. Furthermore, by appropriately modifying the adaptive algorithm we are able to construct efficient approximations, not only

to the exact solution  $u$ , but also to observables (1.3) and (1.4) of problem (4.1)-(4.2). As already mentioned, for small values of  $\varepsilon$  it is very difficult to approximate correctly (1.3) and (1.4), unless very fine mesh sizes are used. The problem becomes harder in cases where caustics develop. This is a hard and delicate issue and adaptivity can play an important role to resolve it.

**5.1. The adaptive algorithm.** We consider, modify and further develop the time-space algorithm of [30], introduced first in [28]. We stress out once more that we do not claim that the particular adaptive algorithm is an optimal one. However, it appears to perform well for the problem under consideration and the estimators at hand. In that respect, it is possible to check the efficiency and robustness of the estimators.

We next briefly describe the algorithm we use. To this end, we use  $\mathcal{G}_n$  to indicate the spatial grid at  $t = t_n$ . We also use the notation  $\zeta_0^I := \|u_0 - U^0\| + \eta_{\text{vo}}(U^0)$ . In addition, we can write

$$\begin{aligned} \mathcal{E}_m^{\text{T},0} &:= \max_{1 \leq n \leq m} \zeta_n^{\text{T},0}, & \mathcal{E}_m^{\text{S},0} &:= \max_{0 \leq n \leq m} \zeta_n^{\text{S},0}, \\ \mathcal{E}_m^{\text{T},1} &\leq \max_{1 \leq n \leq m} \zeta_n^{\text{T},1}, & \mathcal{E}_m^{\text{S},j} &\leq \max_{1 \leq n \leq m} \zeta_n^{\text{S},j}, \quad 1 \leq j \leq 3, & \mathcal{E}_m^{\text{C}} &\leq \max_{1 \leq n \leq m} \zeta_n^{\text{C}}, & \mathcal{E}_m^{\text{D}} &\leq \max_{1 \leq n \leq m} \zeta_n^{\text{D}}, \end{aligned}$$

where  $\zeta_n^{\text{T},j}$ ,  $0 \leq j \leq 1$ ,  $\zeta_n^{\text{S},j}$ ,  $0 \leq j \leq 3$ ,  $\zeta_n^{\text{C}}$  and  $\zeta_n^{\text{D}}$  can readily be obtained from (3.1), (3.2), and (3.15)–(3.18). In all computations the constant  $C$ , cf., (3.15), is taken equal to 1 and the involved local time integrals are computed using the midpoint quadrature rule. For  $1 \leq n \leq m \leq N$ , we further define

$$\zeta_n^{\text{T}} := \zeta_n^{\text{T},0} + \zeta_n^{\text{T},1} \quad \text{and} \quad \zeta_n^{\text{S}} := \sum_{j=0}^3 \zeta_n^{\text{S},j} + \zeta_n^{\text{C}} + \zeta_n^{\text{D}},$$

and let  $\text{tol}_\text{S}$  and  $\text{tol}_\text{T}$  denote the tolerances for the local time and space estimators  $\zeta_n^{\text{T}}$  and  $\zeta_n^{\text{S}}$ , respectively. The main steps of the adaptive algorithm are summarized schematically in the pseudocode below.

More precisely, the adaptive algorithm starts by advancing the solution and computing the local space and time estimators. Next, before starting the process of adapting the spatial grid, we perform a time-step refinement, if necessary, based on the local time estimator. We proceed on the spatial adaptation part of algorithm based on the local space estimator: we first mark the elements for refinement and/or coarsening and we adapt the grid appropriately, we recompute the solution and the local space and time estimators. Next we perform another time-step refinement, if necessary, based on the local time estimator and then we loop back to the space estimator check. One step of the adaptive algorithm then concludes by a time-step coarsening step.

Reasonable choices for the parameters  $\theta_1$  and  $\theta_2$  are  $\theta_1 = 0.9$  and  $\theta_2 = 0.2$ , while for  $\delta_1$  and  $\delta_2$  we take  $\delta_1 = 0.75$  and  $\delta_2 = 1.25$ . In all of the experiments, the coarsening percentage is taken to be 10%. For the mesh refinement percentage, we take 1% for the time-dependent potentials and 5% for all the other cases. In the sequel, we denote by  $\tilde{\mathcal{E}}_m^{\text{T}}$  and  $\tilde{\mathcal{E}}_m^{\text{S}}$  the following global time and space estimators:

$$\tilde{\mathcal{E}}_m^{\text{T}} := \mathcal{E}_m^{\text{T},0} + \max_{1 \leq n \leq m} \zeta_n^{\text{T},1} \quad \text{and} \quad \tilde{\mathcal{E}}_m^{\text{S}} := \zeta_0^I + \mathcal{E}_m^{\text{S},0} + \sum_{j=1}^3 \max_{1 \leq n \leq m} \zeta_n^{\text{S},j} + \max_{0 \leq n \leq m} \zeta_n^{\text{C}} + \max_{0 \leq n \leq m} \zeta_n^{\text{D}},$$

respectively. Finally, we define the total degrees of freedom of the adaptive algorithm at the final time  $T$  as

$$\text{Total DoF's} := \left[ \sum_{n=1}^N k_n M_n \right] + 1,$$

where  $\left[ \cdot \right]$  denotes the integral part of a real number and  $M_n$  denotes the degrees of freedom at time-level  $t_n$ .

**5.2. Time-independent potentials.** For the first set of the numerical experiments with adaptivity, we consider two characteristic cases of time-independent potentials: a constant potential and a harmonic oscillator. In both cases, we consider the WKB initial data (4.2) with

$$(5.1) \quad \sqrt{n_0(x)} = e^{-\lambda^2(x-0.5)^2}, \quad S_0(x) = -\frac{1}{\lambda} \ln \left( e^{\lambda(x-0.5)} + e^{-\lambda(x-0.5)} \right).$$

In particular we consider:

CASE 1:  $[a, b] \times [0, T] = [0, 1] \times [0, 0.1]$ ,  $V(x) \equiv 10$ ,  $\varepsilon = 10^{-4}$  and  $\lambda = 30$ .

CASE 2:  $[a, b] \times [0, T] = [-1, 2] \times [0, 0.54]$ ,  $V(x) = \frac{x^2}{2}$ ,  $\varepsilon = 10^{-3}$  and  $\lambda = 5$ .

For the first case, we discretize in space by B-splines of degree 4. The particular example is interesting, because caustics are formed before the final time  $T = 0.1$ . We first apply the time-space adaptive algorithm.



**Time-Space Adaptive Algorithm**


---

```

1 Choose Parameters :  $\text{tol}_S, \text{tol}_T, \delta_1 \in (0, 1), \delta_2 > 1, \theta_1 \in (0, 1), \theta_2 \in (0, \theta_1)$ 
2 Initialization:
3   Given an initial grid  $\mathcal{G}_0$  compute  $U^0, \zeta_0^I, \zeta_0^{S,0}$ 
4    $\mathcal{G}_0 := \text{AdaptInitialGrid}(U^0, \zeta_0^I, \zeta_0^{S,0}), t = 0$ 
5 while  $t < T$  do
6   At  $t_{n-1}$  given  $(\mathcal{G}_{n-1}, k_{n-1}, U^{n-1})$  set  $\mathcal{G}_n := \mathcal{G}_{n-1}, k_n := k_{n-1}, t_n := t_{n-1} + k_n$ 
7   Solve the discrete problem:  $(\mathcal{G}_{n-1}, U^{n-1}) \rightarrow (\mathcal{G}_n, U^n)$ 
8   Compute Estimators  $\zeta_n^S, \zeta_n^T$  on  $\mathcal{G}_n$ 
9   while  $\zeta_n^T > \theta_1 \text{tol}_T$  do
10     $k_n := \delta_1 k_{n-1}$ 
11     $t_n := t_{n-1} + k_n$ 
12    Solve the discrete problem:  $(\mathcal{G}_{n-1}, U^{n-1}) \rightarrow (\mathcal{G}_n, U^n)$ 
13    Compute Estimators  $\zeta_n^S, \zeta_n^T$  on  $\mathcal{G}_n$ 
14  end
15  while  $\zeta_n^S > \text{tol}_S$  do
16    Mark Elements for Refinement and/or Coarsening
17    if elements are marked then
18      Adapt grid  $\mathcal{G}_n$ 
19      Solve the discrete problem:  $(\mathcal{G}_{n-1}, U^{n-1}) \rightarrow (\mathcal{G}_n, U^n)$ 
20      Compute Estimators  $\zeta_n^S, \zeta_n^T$  on  $\mathcal{G}_n$ 
21    end
22    while  $\zeta_n^T > \theta_1 \text{tol}_T$  do
23       $k_n := \delta_1 k_{n-1}$ 
24       $t_n := t_{n-1} + k_n$ 
25      Solve the discrete problem:  $(\mathcal{G}_{n-1}, U^{n-1}) \rightarrow (\mathcal{G}_n, U^n)$ 
26      Compute Estimators  $\zeta_n^S, \zeta_n^T$  on  $\mathcal{G}_n$ 
27    end
28  end
29  if  $\zeta_n^T \leq \theta_2 \text{tol}_T$  then
30     $k_n := \delta_2 k_n$ 
31  end
32   $t := t_n$ 
33 end

```

---

As expected, we observe adaptivity in space but we do not observe adaptivity in time. However, in this case, we emphasize that regardless of the initial choice of the time-step, the adaptive algorithm is able to produce the required time-step for the desirable tolerance of the error. For this example, the given initial time-step was  $10^{-3}$  and adapted by the algorithm to  $1.34 \times 10^{-7}$ , which is in agreement with (4.8) (see also (4.9)). Next, we perform the same experiment, but using uniform partitions and the same degrees of freedom as in the adaptive algorithm. The estimators are plotted in Figure 1 in logarithmic scale, for both the adaptive algorithm and the uniform partition. We observe that the total estimator computed with the uniform partition is two orders of magnitude larger compared to the corresponding one using adaptivity. Since the time-step, after its initial adaptation remains fixed, the evolution of the total time estimator is the same for both the adaptive algorithm and the corresponding uniform partition. The total space estimator dominates the time estimator in the uniform partition, and this is the reason that  $\tilde{\mathcal{E}}_m^S$  coincides with the total estimator on the right plot of Figure 1.

For the second case, we discretize in space by cubic B-splines and we apply again the adaptive algorithm. As initial time-step we take again  $10^{-3}$  and adapted to  $7.5 \times 10^{-5}$ , which is larger than the expected one. This is

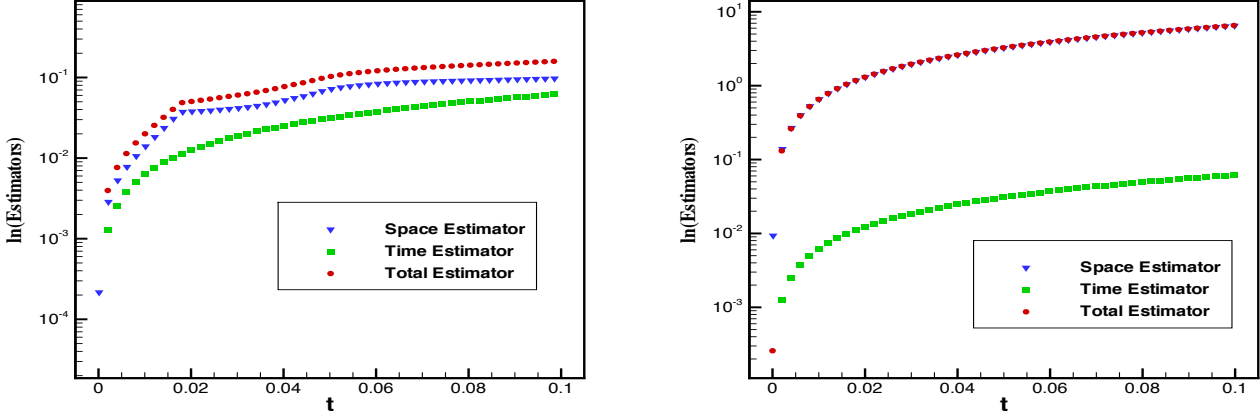


FIGURE 1. Evolution of  $\tilde{\mathcal{E}}_m^T, \tilde{\mathcal{E}}_m^S$  and total estimator in logarithmic scale, using adaptivity (left) and uniform partitions with the same degrees of freedom (right) for the case  $V(x) \equiv 10$ .

because both (4.8), (4.9) are sufficient, but not always necessary conditions for convergence for problem (4.1)–(4.2). The fact that the adaptive algorithm is able to compute the correct time-step size can be considered an advantage, since for the linear Schrödinger equation in the semiclassical regime such a choice is crucial and delicate from the point of view of accuracy and stability of the approximations, as well as from the point of view of computational cost. In each time-slot, the mesh size varies from  $7.32 \times 10^{-6}$  to  $2.4 \times 10^{-1}$ , which proves that conditions (4.7) can be relaxed through adaptivity in space; very fine mesh sizes are needed only in certain areas of  $[-1, 2]$ . In Figure 2, we plot the evolution of time, space and total estimators in logarithmic scale and the position density at the beginning and at the final time  $T = 0.54$ . As we observe from the plot of  $|U|^2$  at  $T = 0.54$ , caustics are formed for this problem as well. The a priori knowledge of such information requires very technical and tedious calculations. However this information can be obtained through the a posteriori error analysis and adaptivity.

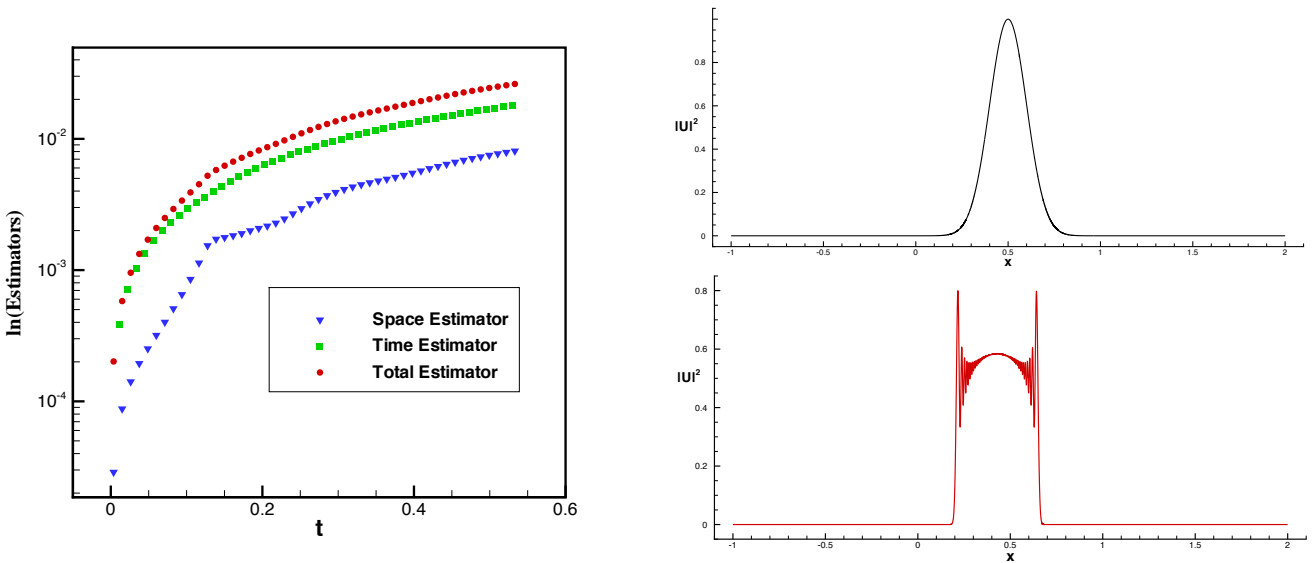


FIGURE 2. Evolution of  $\tilde{\mathcal{E}}_m^T, \tilde{\mathcal{E}}_m^S$  and total estimator in logarithmic scale, using the adaptive algorithm (left) and position density for  $t_0 = 0$  (upper right) and at the final time  $T = 0.54$  (lower right) for the harmonic oscillator.

**5.3. Time-dependent potentials.** The simplest time-dependent potentials are of the form  $V(x, t) = \frac{x^2}{2}\omega(t)$ , where  $\omega$  denotes a smooth function in time; [8, 22]. To check the efficiency of the estimators during time adaptivity, we choose two time-dependent potentials of this form, which change relatively fast with time.

For the first experiment, we solve in  $[a, b] \times [0, T] = [1, 2] \times [0, 3]$  and we take  $V(x, t) = \frac{x^2}{2} \cdot \frac{1}{10t + 0.05}$  and  $\varepsilon = 10^{-2}$ . As  $\sqrt{n_0(x)}$  we take the one in (5.1), while we choose  $S_0(x) = 5(x^2 - x)$ , and we define the initial condition through (4.2). We use quadratic B-splines and we apply the time-space adaptive algorithm. In Figure 3, we plot the evolution of the estimators in a logarithmic scale, as well as the variation of the time-steps  $k_n$  during time adaptivity. The considered potential changes faster with time in the subinterval  $[0, 1]$ , compared to  $[1, 3]$ , and this is the reason the required time-step is considerably smaller in this area. For this experiment, in each time-slot, the mesh size varies from  $1.17 \times 10^{-4}$  to  $1.2 \times 10^{-1}$ .

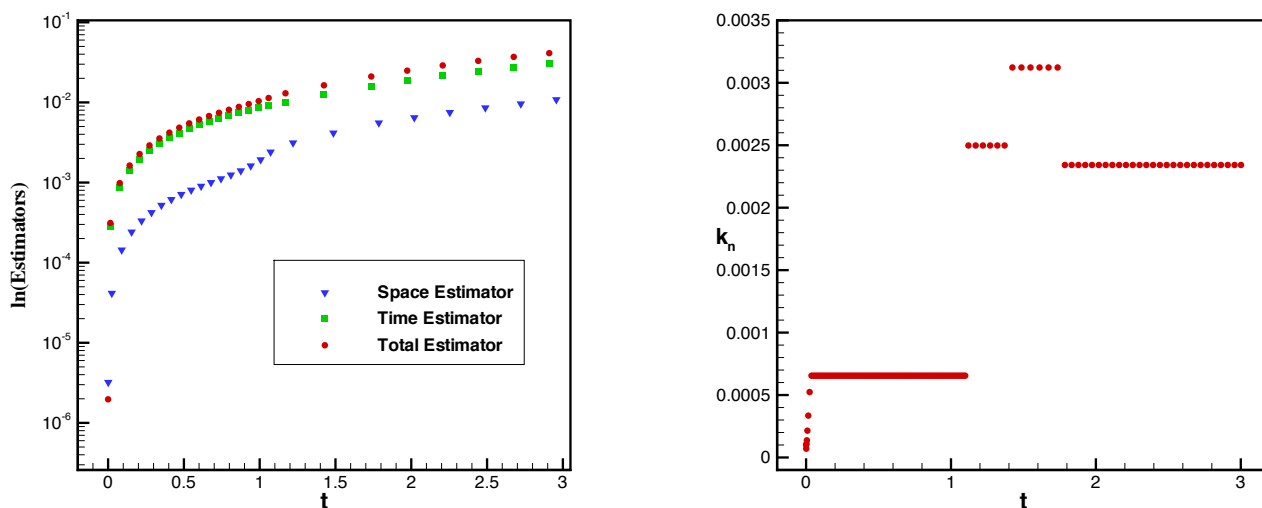


FIGURE 3. Evolution of  $\tilde{\mathcal{E}}_m^T, \tilde{\mathcal{E}}_m^S$  and the total estimator in logarithmic scale (left), and variation of time-steps  $k_n$  during adaptivity (right), for  $V(x, t) = \frac{x^2}{2} \cdot \frac{1}{10t + 0.05}$ .

For the second experiment, we solve in  $[a, b] \times [0, T] = [-1, 2] \times [0, 1]$  and we take  $V(x, t) = \frac{x^2}{2} \cdot \frac{1}{t + 0.05}$  and  $\varepsilon = 2.5 \times 10^{-3}$ . We take the same initial condition as in the previous experiment and cubic B-splines. In Figure 4, we plot the evolution of the estimators in logarithmic scale and the variation in time of the time-steps and of the degrees of freedom. This is a characteristic example where intensive adaptivity is observed, in both time and space.

In Figure 5, we plot four snapshots: at the beginning, at the final time and in two intermediate times. From the plots we can also see the distribution of the grid points. At  $t = 0$ , we start with uniform partition. For the remaining three snapshots, we observe that the points are dense close to rough changes of the approximation. Especially, in the third snapshot (left plot from below), almost all the points are concentrated close to the peak, while in areas where the solution doesn't change much, the grid is very sparse. This is an indicator of the robustness of the adaptive algorithm which can provide reliable results with considerably less computational cost, compared to uniform grids.

**5.4. Approximation of the observables.** We focus next on the approximation of the observables (1.3), (1.4). In particular, we propose a modification of the adaptive algorithm and we verify numerically the advantages of the modified algorithm for the approximation of the observables, in terms of computational cost and accuracy.

For CNFE schemes, it is well known that the restrictive conditions between mesh sizes and the parameter  $\varepsilon$  needed for the efficient error control of the exact solution of (4.1)–(4.2) can be relaxed for the error control of

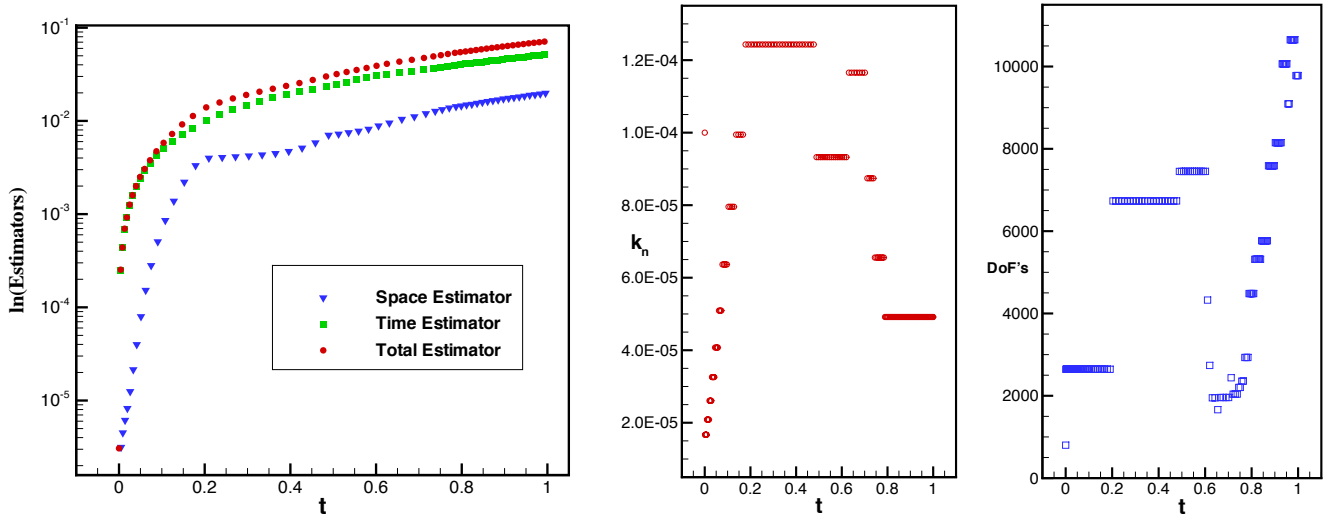


FIGURE 4. Evolution of estimators in logarithmic scale (left) and variation of the time-steps  $k_n$  and the DoF's versus  $t$  (right) during adaptivity for  $V(x, t) = \frac{x^2}{2} \cdot \frac{1}{t+0.05}$ .

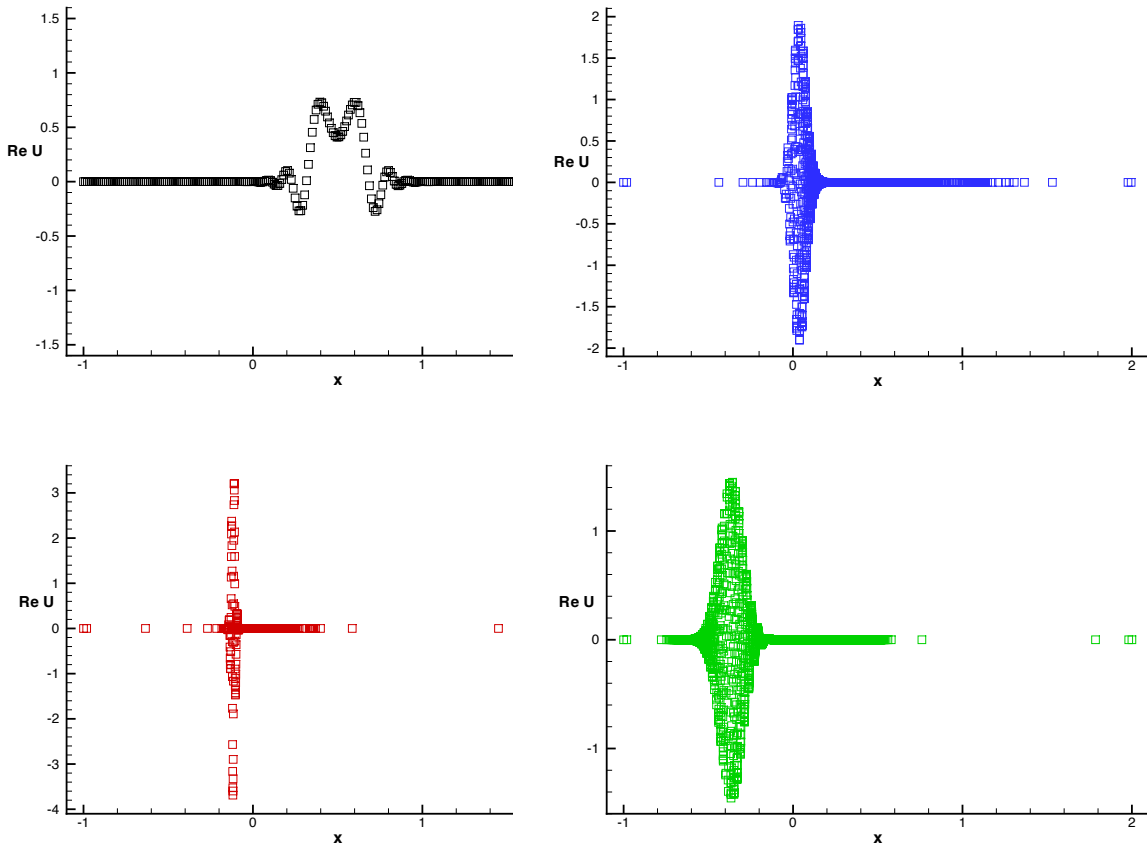


FIGURE 5. Snapshots of the real part of the approximation and distribution of the grid points for the case  $V(x, t) = \frac{x^2}{2} \cdot \frac{1}{t+0.05}$ .

the corresponding observables. More precisely, as it was proven in [26, 27], a sufficient and necessary condition for approximating well the observables is  $\frac{h}{\varepsilon} + \frac{k}{\varepsilon} \rightarrow 0$ . Moreover, the  $L^\infty(L^2)$  approximation of the exact solution implies the  $L^\infty$  approximation of observables' mean value; [2]. In view of all these, we modify the adaptive algorithm as follows: We multiply all estimators but  $\mathcal{E}_m^{S,0}$  and  $\mathcal{E}_m^{T,0}$  by  $\varepsilon$ , so that the new estimators will converge provided that  $\frac{h}{\varepsilon} + \frac{k}{\varepsilon} \rightarrow 0$ , cf., (4.7),(4.8). Then, we apply the same algorithm, but with respect to these new estimators.

We then perform various numerical experiments to verify whether this partially heuristic idea can be advantageous to the approximation of the observables. More precisely, we consider the constant potential  $V(x) \equiv 10$  and the WKB initial condition (4.2) with  $\sqrt{n_0}$  and  $S_0$  as in (5.1). We perform the experiments with adaptivity only in space. For the first two tests, we take  $[a, b] \times [0, T] = [-1, 2] \times [0, 0.54]$ ,  $\lambda = 5$  and  $\varepsilon = 10^{-3}$  or  $\varepsilon = 2.5 \times 10^{-4}$ . Recall that the particular example, considered earlier in [2], is interesting because caustics are formed before the final time. For the case  $\varepsilon = 10^{-3}$ , we take  $k = 10^{-5}$  and discretize by quadratic B-splines, whereas for  $\varepsilon = 2.5 \times 10^{-4}$ , we take  $k = 3 \times 10^{-6}$  and discretize by B-splines of degree 4. In Figures 6, 8, we plot the position density using the adaptive algorithm (left plot) and uniform grid with the same degrees of freedom (right plot). The solid line corresponds to the semiclassical limit of the exact observable which is possible to compute for constant potentials. The dotted lines correspond to the approximate observable. As we observe from these plots, the approximation using adaptivity is very good, while the one using uniform partition misses completely the angles and peaks. Similar comments can be made for the plots referring to the current density. These plots can be viewed in Figures 7 and 9 for  $\varepsilon = 10^{-3}$  and  $2.5 \times 10^{-4}$ , respectively. In the plots concerning the approximations with space adaptivity, we also see the distribution of the grid points. It is remarkable that most of the points are concentrated close to the angles and peaks. On the contrary, very few points are placed around the endpoints, where the observables remain constant. The total number of degrees of freedom in adaptivity corresponds to 1458 DoF's in each time-slot for  $\varepsilon = 10^{-3}$  and to 3186 for the case  $\varepsilon = 2.5 \times 10^{-4}$ . The required degrees of freedom in each time-slot with uniform partition are more than 3000 for  $\varepsilon = 10^{-3}$  and more than 12000 for  $\varepsilon = 2.5 \times 10^{-4}$ .

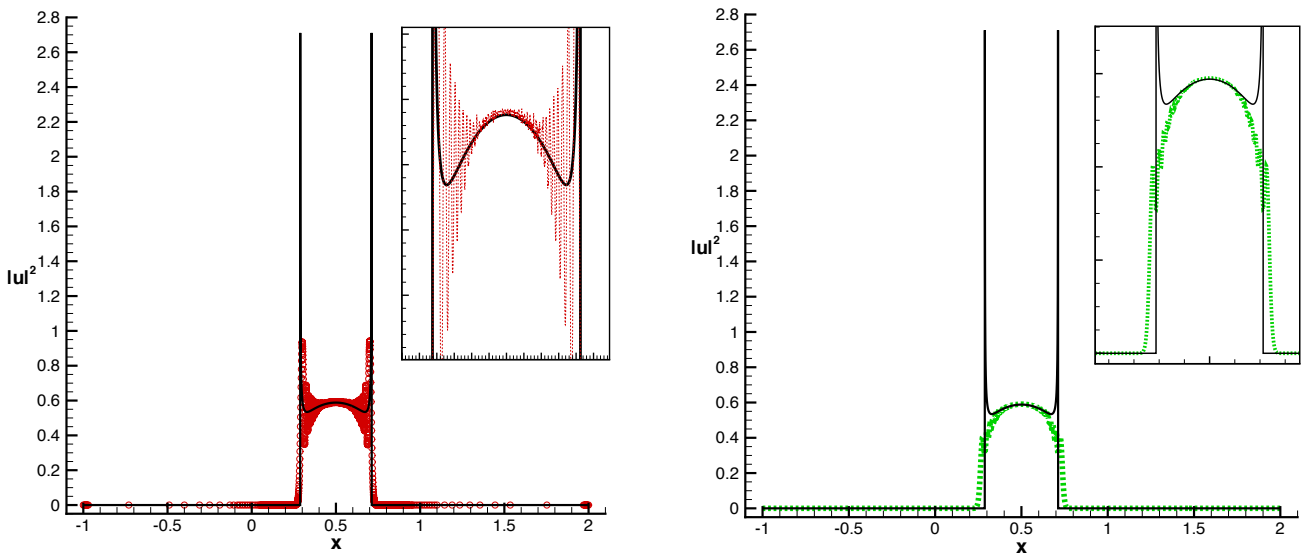


FIGURE 6. Position density at the final time  $T = 0.54$  in case  $\varepsilon = 10^{-3}$ . Solid line represents the semiclassical limit of the exact observable, while dotted line represents the approximation using adaptivity (left) and uniform partition with the same DoF's (right).

For the first two tests, we take  $[a, b] \times [0, T] = [-1, 2] \times [0, 0.54]$ ,  $\lambda = 5$  and  $\varepsilon = 10^{-3}$  or  $\varepsilon = 2.5 \times 10^{-4}$ . Recall that the particular example, considered earlier in [2], is interesting because caustics are formed before the final time. For the case  $\varepsilon = 10^{-3}$ , we take  $k = 10^{-5}$  and discretize by quadratic B-splines, whereas for

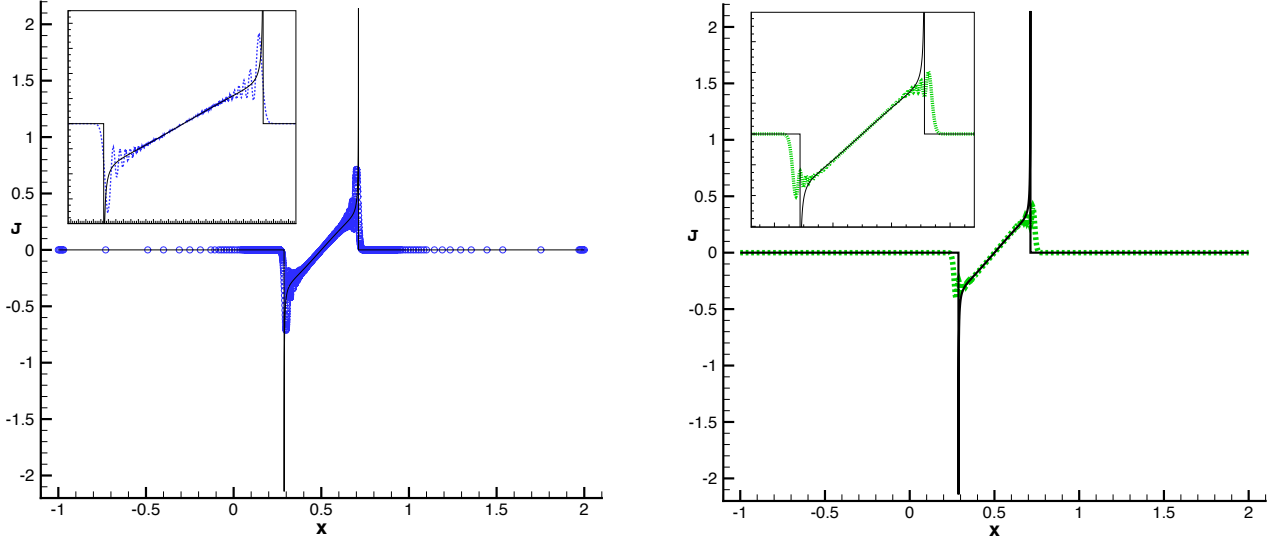


FIGURE 7. Current density at the final time  $T = 0.54$  in case  $\varepsilon = 10^{-3}$ . Solid line represents the semi-classical limit of the exact observable, while dotted line represents the approximation using adaptivity (left) and uniform partition with the same DoF's (right).

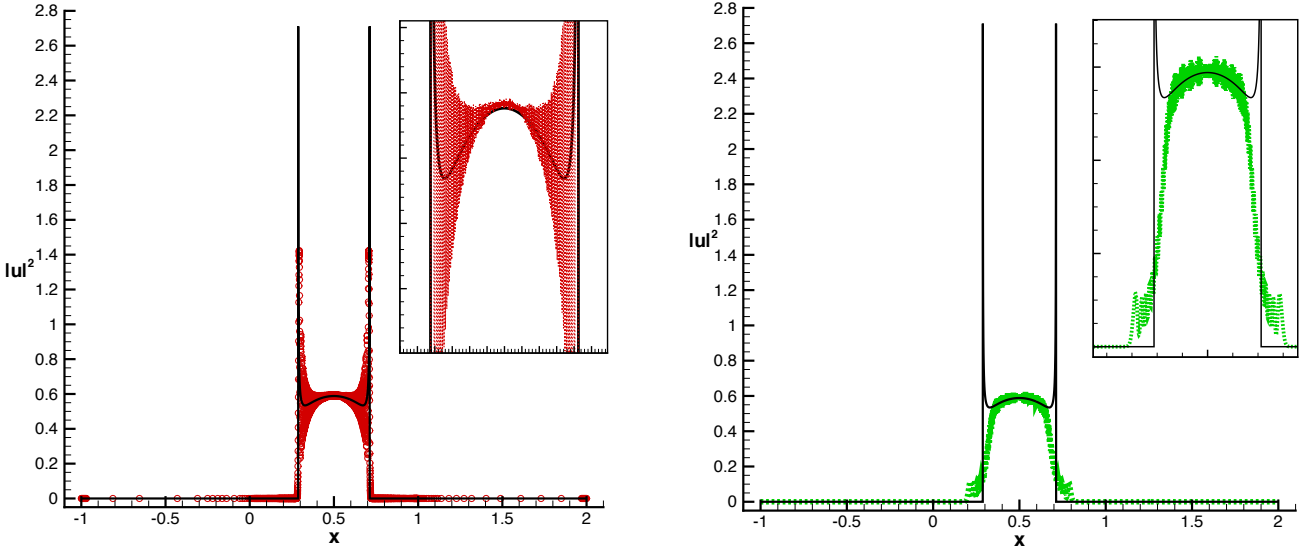


FIGURE 8. Position density at the final time  $T = 0.54$  in case  $\varepsilon = 2.5 \times 10^{-4}$ . Solid line represents the semiclassical limit of the exact observable, while dotted line represents the approximation using adaptivity (left) and uniform partition with the same DoF's (right).

$\varepsilon = 2.5 \times 10^{-4}$ , we take  $k = 3 \times 10^{-6}$  and discretize by B-splines of degree 4. In Figures 6, 8, we plot the position density using the adaptive algorithm (left plot) and uniform grid with the same degrees of freedom (right plot). The solid line corresponds to the semiclassical limit of the exact observable which is possible to compute for constant potentials. The dotted lines correspond to the approximate observable. As we observe from these plots, the approximation using adaptivity is very good, while the one using uniform partition misses completely the angles and peaks. Similar comments can be made for the plots referring to the current density. These plots can be viewed in Figures 7 and 9 for  $\varepsilon = 10^{-3}$  and  $2.5 \times 10^{-4}$ , respectively. In the plots concerning the approximations with space adaptivity, we also see the distribution of the grid points. It is remarkable that most of the points are concentrated close to the angles and peaks. On the contrary, very few points are placed around the endpoints, where the observables remain constant. The total number of degrees of freedom in adaptivity corresponds to 1458 DoF's in each time-slice for  $\varepsilon = 10^{-3}$  and to 3186 for the case  $\varepsilon = 2.5 \times 10^{-4}$ .

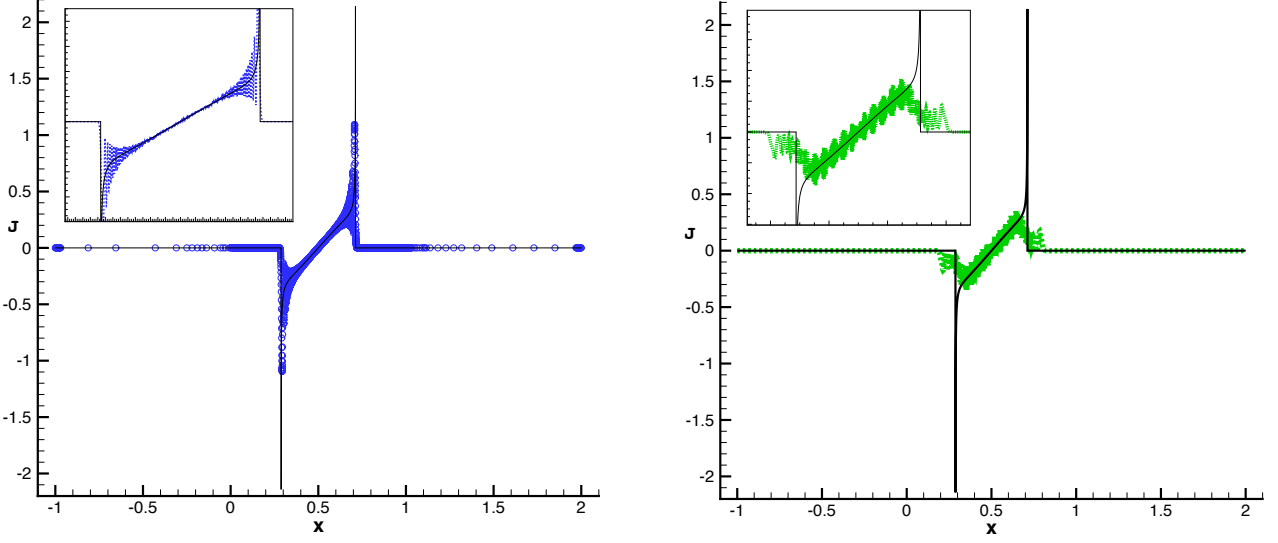


FIGURE 9. Current density at the final time  $T = 0.54$  in case  $\varepsilon = 2.5 \times 10^{-4}$ . Solid line represents the semiclassical limit of the exact observable, while dotted line represents the approximation using adaptivity (left) and uniform partition with the same DoF's (right).

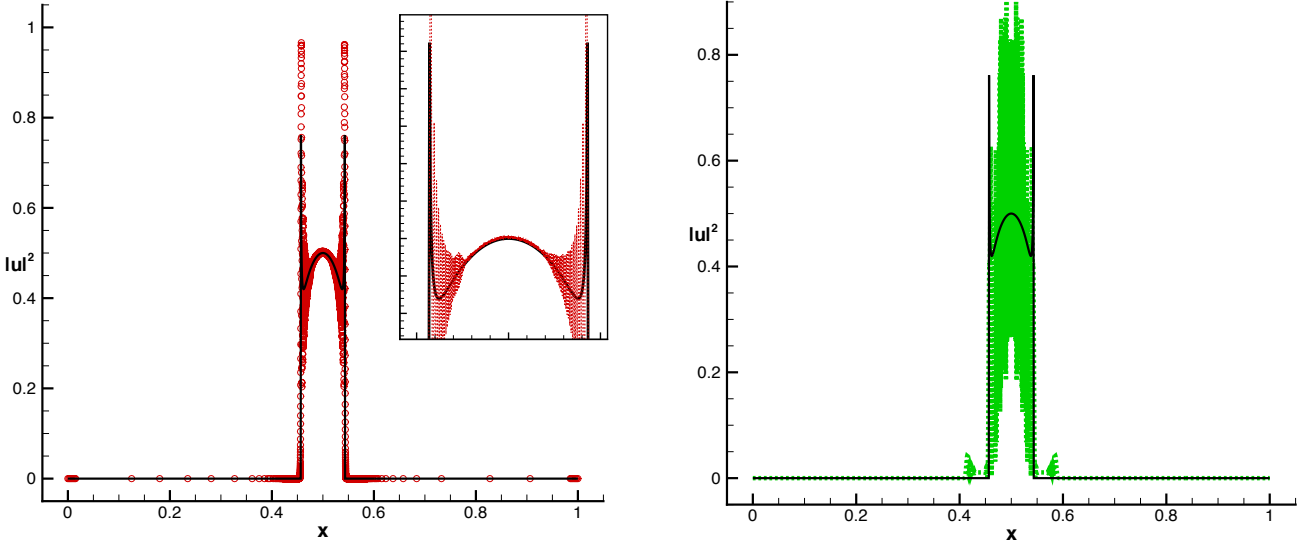


FIGURE 10. Position density at the final time  $T = 0.1$  in case  $\varepsilon = 5 \times 10^{-5}$ . Solid line represents the semiclassical limit of the exact observable, while dot line represents the approximation using adaptivity (left) and uniform partition with the same DoF's (right).

The required degrees of freedom in each time-slot with uniform partition are more than 3000 for  $\varepsilon = 10^{-3}$  and more than 12000 for  $\varepsilon = 2.5 \times 10^{-4}$ .

The first two tests indicate that the smaller the value of  $\varepsilon$  using adaptivity is very advantageous. To make this indication stronger, we perform a final test in which  $[a, b] \times [0, T] = [0, 1] \times [0, 0.1]$ ,  $\lambda = 30$  and  $\varepsilon = 5 \times 10^{-5}$ . This is another example where caustics are formed. We use cubic B-splines and  $k = 5 \times 10^{-7}$ .

In Figures 10,11, we plot on the left the approximation with space adaptivity and on the right the corresponding with uniform partition and the same degrees of freedom. The result obtained using the uniform partition is very poor. The approximate solution misses the angles and peaks, and, in fact, fails to approximate the actual observables. On the other hand, those obtained by adaptivity, appear to be very good approximations. The number of total degrees of freedom in adaptivity corresponds to 3670 DoF's in each time-slot, while the required DoF's in each time slot with uniform partition is more than 20000.

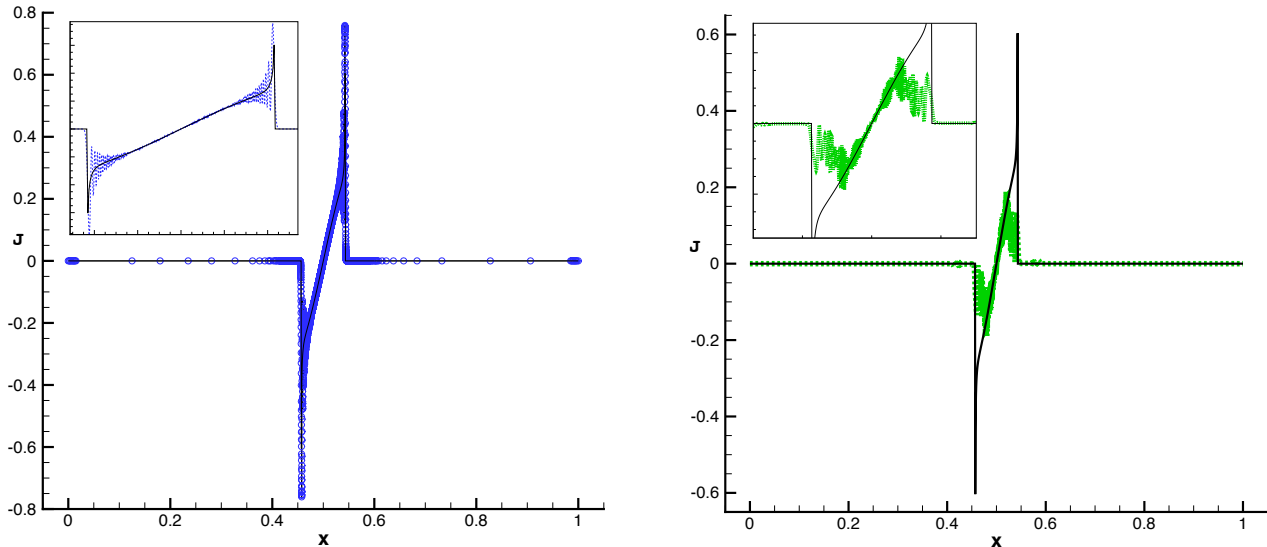


FIGURE 11. Position density at the final time  $T = 0.1$  in case  $\varepsilon = 5 \times 10^{-5}$ . Solid line represents the semiclassical limit of the exact observable, while dotted line represents the approximation using adaptivity (left) and uniform partition with the same DoF's (right).

This final set of experiments, indicates that the a posteriori error estimators can appropriately be used together with adaptive strategies not only for the efficient error control of the wave function  $u$ , but for the observables as well. The tests suggest that the computational cost is drastically reduced and the adaptive procedure gives encouraging results for small values of the Planck constant  $\varepsilon$ . However, no rigorous analysis has been provided and further numerical experiments including more general potentials need to be performed in order to draw safe conclusions. This very interesting problem requires further investigation and will be the subject of a forthcoming work.

#### ACKNOWLEDGMENTS

Some of the ideas of the theoretical part of the paper are taken from second author's Ph.D Thesis, [19]. I.K. is grateful to her Ph.D advisor, Prof. Charalambos Makridakis for suggesting the problem and for his academic guidance and support. The authors thank Prof. Georgios Akrivis for many helpful remarks.

#### REFERENCES

- [1] G. Akrivis, Ch. Makridakis, R. H. Nochetto, *A posteriori error estimates for the Crank-Nicolson method for parabolic equations*, Math. Comp. **75** (2006) 511–531.
- [2] W. Bao, S. Jin, P. A. Markowich, *On time-splitting spectral approximations for the Schrödinger equation in the semiclassical regime*, J. Comput. Phys. **175** (2002), 487–524.
- [3] Ch. Besse, *A relaxation scheme for the nonlinear Schrödinger equation*, SIAM J. Numer. Anal. **42** (2004) 934–952.
- [4] S.C. Brenner, L.R. Scott, *The Mathematical Theory of Finite Element Methods*, 2<sup>nd</sup> edition, Springer, NewYork, 2002.
- [5] E. Bänsch, F. Karakatsani, Ch. Makridakis, *A posteriori error control for fully discrete Crank-Nicolson schemes*, SIAM J. Numer. Anal. **50** (2012) 2845–2872.
- [6] E. Bänsch, F. Karakatsani, Ch. Makridakis, *The effect of mesh modification in time on the error control of fully discrete approximations for parabolic equations*, to appear in Appl. Numer. Math., doi:10.1016/j.apnum.2011.08.008.
- [7] A. Cangiani, E.H. Georgoulis, S. Metcalfe, *An a posteriori error estimator for discontinuous Galerkin methods for non-stationary convection-diffusion problems*. Submitted for publication.
- [8] P. Camiz, A. Gerardi, C. Marchioro, E. Presutti, E. Scacciatelli, *Exact solution of a time-dependent quantal harmonic oscillator with a singular perturbation*, J. Mathematical Phys. **12** (1971) 2040–2043.
- [9] Z. Chen, J. Feng, *An adaptive finite element algorithm with reliable and efficient error control for linear parabolic problems*, Math. Comp. **73** (2004) 1167–1193.
- [10] Ch. Clément, *Approximation by finite element functions using local regularization*, Analyse Numérique **9** (1975) 77–84.
- [11] R. Dautray, J.-L. Lions, *Mathematical Analysis and Numerical Methods for Science and Technology*, vol. 5, Evolution Problems I, 2<sup>nd</sup> edition, Springer-Verlag, Berlin, 2000.
- [12] A. Demlow, O. Lakkis, Ch. Makridakis, *A posteriori error estimates in the maximum norm for parabolic problems*, SIAM J. Numer. Anal. **47** (2009) 2157–2176.
- [13] W. Dörfler, *A time- and space-adaptive algorithm for the linear time-dependent Schrödinger equation*, Numer. Math. **73** (1996) 419–448.



- [14] M.D. Feit, J.A. Fleck Jr., A. Steiger, *Solution of the Schrödinger equation by a spectral method*, J. Comput. Phys. **47** (1982) 412–433.
- [15] E. Georgoulis, O. Lakkis, Ch. Makridakis, *A posteriori  $L^\infty(L^2)$ -error bounds in finite element approximation of the wave equation*. Submitted for publication.
- [16] P. Gérard, P. A. Markowich, N. J. Mauser, and F. Poupaud, *Homogenization limits and Wigner transforms*, Comm. Pure Appl. Math. **50**, (1997), 323–379.
- [17] Ch. Kreuzer, C.A. Möller, A. Schmidt, K.G. Siebert: *Design and convergence analysis for an adaptive discretization of the heat equation*, IMA J. Numer. Anal., doi: 10.1093/imanum/drr026 .
- [18] I. Kyza, *A posteriori error analysis for the Crank-Nicolson method for linear Schrödinger equations*, ESAIM Math. Model. Numer. Anal. **45** (2011) 761–778.
- [19] I. Kyza, *A posteriori error estimates for approximations of semilinear parabolic and Schrödinger-type equations*, PhD Thesis, University of Crete, 2009.
- [20] I. Kyza, Ch. Makridakis, M. Plexousakis, *Error control for time-splitting spectral approximations of the semiclassical Schrödinger equation*, IMA J. Numer. Anal. **31** (2011) 416–441.
- [21] O. Lakkis, Ch. Makridakis, *Elliptic reconstruction and a posteriori error estimates for fully discrete linear parabolic problems*, Math. Comp. **75** (2006) 1627–1658.
- [22] P.G.L. Leach, *Invariants and wavefunctions for some time-dependent harmonic oscillator type Hamiltonians*, J. Mathematical Phys. **18** (1977) 1902–1907.
- [23] A. Lozinski, M. Picasso, V. Prachittham, *An anisotropic error estimator for the Crank-Nicolson method: Application to a parabolic problem*, SIAM J. Sci. Comput. **31** (2009) 2757–2783.
- [24] Ch. Makridakis, R.H. Nochetto, *Elliptic reconstruction and a posteriori error estimates for parabolic problems*, SIAM J. Numer. Anal. **41** (2003) 1585–1594.
- [25] M.M.H. Mansour, W.J.H. Müller-Kirsten, *Perturbative technique as an alternative to the WKB method applied to the double-well potential*, J. Math. Phys. **23** (1982)1835–1845.
- [26] P.A. Markowich, P. Pietra, C. Pohl, *Numerical approximation of quadratic observables of Schrödinger-type equations in the semi-classical limit*, Numer. Math. **81** (1999), 595–630.
- [27] P.A. Markowich, P. Pietra, C. Pohl, H.-P. Stimming, *A Wigner-measure analysis of the Dufort-Frankel scheme for the Schrödinger equation*, SIAM J. Numer. Anal.**40** (2002) 1281–1310.
- [28] R.H. Nochetto, A. Schmidt, C. Verdi, *A posteriori error estimation and adaptivity for degenerate parabolic problems*, Math. Comp. **69** (2000) 1–24.
- [29] G.A. Pozzi, *Problemi di Cauchy e problemi ai limiti per equazioni di evoluzione del tipo di Schroedinger lineari e non lineari. I. L'equazione lineare astratta*, (Italian), Ann. Mat. Pura Appl. **78** (1968) 197–258.
- [30] A. Schmidt, K.G. Siebert, *Design of adaptive finite element software. The finite element toolbox ALBERTA*, Lecture Notes in Computational Science and Engineering, **42**, Springer-Verlag, Berlin, 2005.
- [31] B. Simon, *Semiclassical analysis of low lying eigenvalues. II. Tunneling*, Ann. of Math.(2) **120** (1984), 89–118.
- [32] L.R. Scott, S. Zhang, *Finite element interpolation of non-smooth functions satisfying boundary conditions*, Math. Comp. **54** (1990) 483–493.
- [33] R. Verfürth, *A posteriori error estimates for finite element discretizations of the heat equation*, Calcolo **40** (2003) 195–212.

(Theodoros Katsaounis) DEPARTMENT OF APPLIED MATHEMATICS, UNIVERSITY OF CRETE, 71409 HERAKLION-CRETE, GREECE, and INSTITUTE OF APPLIED AND COMPUTATIONAL MATHEMATICS,, FORTH, VASSILIKA VOUTON, GR 700 13 HERAKLION-CRETE, GREECE

*E-mail address:* thodoros@tem.uoc.gr

(Irene Kyza) INSTITUTE OF APPLIED AND COMPUTATIONAL MATHEMATICS, FOUNDATION OF RESEARCH & TECHNOLOGY-HELLAS, NIKOLAOU PLASTIRA 100, VASSILIKA VOUTON, GR 700 13 HERAKLION-CRETE, GREECE

*E-mail address:* kyza@iacm.forth.gr